Development of High-Throughput Platforms for Single-Cell Analysis

by

Denis Loginov

B.Sc., M.Sc. Applied Physics and Mathematics

Moscow Institute of Physics and Technology

Submitted to the Department of Materials Science and Engineering in partial fulfillment of the requirements for the degree of

Master of Science in Materials Science and Engineering

at the

MASSACHUSETTS INSTITUTE OF TECHNOLOGY

February 2015

Signature of Author: _____

Department of Materials Science and Engineering
September 25, 2014

Certified by: _____

J. Christopher Love
Associate Professor of Chemical Engineering
Thesis Supervisor

Certified by: _____

Darrell J. Irvine
Professor of Materials Science and Engineering
and Biological Engineering
Thesis Co-Advisor

Accepted by: _____

Donald Sadoway
Chair, Departmental Committee on Graduate Students

Development of High-Throughput Platforms for Single-Cell Analysis

by

Denis Loginov

Submitted to the Department of Materials Science and Engineering
on September 25, 2014 in partial fulfillment of the requirements
for the degree of Master of Science in
Materials Science and Engineering

Abstract

Many important areas of research regarding human health, such as immunology and cancer biology, deal with highly heterogeneous populations of cells where the contributions of individual players cannot be ignored. Single-cell technologies aim to resolve this heterogeneity by analyzing many individual cells in a high-throughput manner. Here we developed two examples of such tools that rely on microfabricated arrays of microwells. The first platform merges fluorescence cytometry with label-free profiling of the small molecule composition of tens of thousands of cells based on matrix-assisted laser desorption/ionization (MALDI) mass spectrometry. We evaluated several materials and approaches to chip fabrication suitable for interfacing with a MALDI instrument. We also developed an analytical pipeline for efficient processing of cells on the chip and demonstrated its application to the analysis of brain tumor samples. The second platform provides a new format of microwell arrays for fluorescence cytometry that improves their compatibility with a range of automated equipment and enables more efficient processing of a greater number of samples, while preserving viability and identity of cells for subsequent analyses. We demonstrated its utility for on-chip enrichment and recovery of circulating tumor cells (CTCs) and high-content immunophenotyping of small clinical samples.

Thesis Supervisor: J. Christopher Love
Title: Associate Professor of Chemical Engineering

Thesis Co-Advisor: Darrell J. Irvine
Title: Professor of Materials Science and Engineering and Biological Engineering

Acknowledgements

I would like to thank my advisors Professor J. Christopher Love and Professor Darrell J. Irvine, along with my unofficial advisor Professor Nathalie Y. R. Agar, for their enormous support in all my pursuits. Their constant encouragement, patience and willingness to guide my work at any level, both professional and personal, made a tremendous difference.

I would also like to acknowledge all my collaborators in Nathalie's group at BWH that made the first part of this work possible. Special thanks goes to Dr. David Calligaris, Revaz Machaidze, Isaiah Newton, and Dr. Xiaohui Liu for helping me with the different stages of my experiments. Revaz got me started with cell culture and was supportive in other aspects ever since. I would not have gotten far without David's expertise on MALDI imaging and analysis. Isaiah was instrumental in getting computers to do their job. Xiaohui helped with the first proof-of-concept experiments that outlined the prospects of the project.

The second half of my thesis was inspired and made possible by my interactions with Viktor Adalsteinsson at the Love lab. His enormous ability to postulate research problems and find simple solutions, along with assistance in experiments for half of this work, made all the difference. I'd also like to mention the efforts of Mark Kalinich, who helped Viktor and me with the most laborious part of counting cells, along with other experiments. I cannot understate my gratitude to Dr. Todd Gierahn, who developed MuSIC and performed immunophenotyping experiments that I discuss later on. I also thank Todd and Viktor for reviewing this thesis.

In addition, I would like to recognize members of the MTL staff who taught me basic microfabrication techniques that underlined this work: Kurt Broderick, Scott Poesse, Bob Bicchieri and many others were extremely helpful in this regard. Not least, MIT's MTL and ISN provided instrumentation for microfabrication and characterization. In addition, I would especially thank the ISN for financial support. Finally, Dr. Andy Kamholtz provided useful discussions on "where the rubber meets the road" of soft embossing and injection molding.

It is hard to express my personal gratitude to all members of my advisors' labs. Yvonne, Yuan, Debo, Todd, Viktor, Ayca, Brittany, Alex, Rita, Qing, Tim, Alan, the Rachels, the Johns, Lionel, Nick, Kartik, Li-Lun, Brinda, Ross, Mei-Chen, Arnon, Revaz, David, Isaiah, Greg and others not only provided useful tips, general assistance and stimulating thoughts or requests at some point in time, but became my friends at work and often beyond.

Outside of the labs, my friendly classmates Joaquin, Neel, Ami, Akira, Kunal, Mehmet, Alan, Ryan and many others shared the struggles and triumphs of the first year. Joaquin has remained a close friend ever since.

Life as a graduate student at MIT would not be possible without a dedicated residence – Sidney-Pacific – that became the best place to be over these years. Endless interactions with my buddies Ahmed, Amy, Chelsea, Tim, the Georges, Holly, Mirna, Brian and others, as well as the housemasters Marks and Tangs provided the comfort of home away from home.

Last but possibly the most important is unconditional love from my parents. I cannot thank you enough for everything you have done for me throughout my whole life.

Table of Contents

List Of Figures

1. Introduction

1.1 Overview of technologies for single-cell analysis

The last several decades have seen a tremendous progress in our understanding of biological processes. An ever-growing number of assays, made available through highly-automated tools such as quantitative PCR instruments and high-throughput DNA sequencers, have allowed us to uncover molecular mechanisms of these processes in exquisite detail [1].

Despite these advances, research in many important fields, such as immunology and cancer biology, has made it increasingly clear that bulk measurements (i.e. on the level of cell populations and tissue homogenates) can mask characteristics of individual cells or subsets of cells that contribute significantly to biological processes, but may not be identical to the "population average" measured by these techniques. Such heterogeneity appears not only in genetically diverse populations (as in the case of many tumors, or T and B lymphocytes), but also at the clonal level, based on differences in epigenetic states of the cells and stochasticity in cellular signaling [1], [2]. In addition, interactions between individual players may not be resolved if only an "average" behavior is studied. As a result, traditional methods may draw a misleading picture of dynamic responses of cells to the given perturbations, necessitating development of technologies for *single-cell* analysis.

Important classes of measurements include characterization of genotype, proliferation, cell surface markers, secreted molecules and interactions between individual cells [2]. Tracing these parameters for every cell may reveal not only new biology (such as specific pathways and interactions in the immune system), but also inform diagnosis and treatment (for example, based on known mutations in cancer). Although taking *in vivo* measurements would in many cases be preferable to preserve the natural state of cells and their microenvironments, it is often impossible or impractical. *In vitro* measurements are less restrictive, but may also pose limitations on the number and types of assays that may be applied. First, they should offer a means to *isolate*

individual cells for subsequent interrogation. They should also be *sensitive* enough to reliably detect signals associated with each cell. The number of simultaneously detected signals (*multiplexity*) may become another limitation. Some measurements (such as genetic profiling) may be done as an end-point assay, while others (such as functional or phenotypic characteristics) may be *repetitive* due to their *non-destructive* nature. Another important aspect is the *throughput* of any assay, which poses a practical limit on how many measurements and on how many cells can be feasibly done in a given time; methods that process cells in *parallel* may be much more efficient than *serial* ones. No less important is the *number of cells* required for a particular method, which implies the kinds of samples that could be processed with it: while cell lines and animal models are an abundant source of material used in research, clinical samples often barely meet this criterion [2]. In this regard, any method that preserves viability and identity of cells for subsequent analyses (i.e. being *modular*) may provide additional flexibility. Finally, fine control over individual cells and their measurements should be carefully balanced with the overall *simplicity* of the approach, as doing so may drastically affect the costs and labor spent on any analysis.

Optical tools have become a de-facto standard for the majority of measurements in biological research, both at the bulk and the single-cell levels. Indeed, high sensitivity and resolution (down to the single-molecule level) enabled by advanced light sources and detectors – lasers, photomultiplier tubes (PMTs), electron multiplying charge-coupled devices (EMCCDs) etc. (which in turn, resulted from advances in physical sciences and microfabrication) – coupled with the generally non-destructive nature of optical measurements (allowing repeated, time-course and modular experiments) and an ever-growing availability of fluorescent probes, provided a unique framework for studying biological processes not easily achieved with any other physical observations. However, optical measurements still suffer from reduced multiplexity due to the overlapping spectra of the dyes, the requirement for labels specific to target molecules, and oftentimes a necessity to amplify the analytes (such as nucleic acids). As such, a number of

orthogonal methods that complement or substitute fluorescence measurements by relying on alternative physics, have been developed [1]: Raman spectroscopy, mass spectrometry, methods using electric and magnetic fields (capillary electrophoresis (CE), dielectrophoresis (DEP), iso-dielectric separation (IDS)), as well as mechanical forces (acoustic or inertial focusing). All these techniques greatly expand the arsenal of tools available for single-cell analysis, allowing researchers to choose the best set of tools for each case.

While the majority of tools for bulk and even single-cell analysis has traditionally been developed at the "macro" scale, the advancement of technologies for fabrication of microstructures in recent years has enabled production of miniaturized systems, or "lab on a chip" (LoC) devices. These tools utilize the concept of confinement of cells or their lysates and associated reagents to a small volume, often on the order of nanoliters or less. They not only serve to isolate cells from each other, but also increase local concentrations of analytes to achieve higher sensitivity, reduce cost of consumables and time spent on each analysis (often by processing many cells or reactions in parallel or in fast iterations), as well as automate analytical pipelines and reduce potential for human error [1]. Prominent examples include passive [3] and actively actuated [4] microfluidic traps, droplet encapsulation [5] and microwell arrays [6]. Passive devices trap one or a few cells in weir structures and trace their growth or responses to stimuli with fluorescence microscopy [3]; although efficient trapping is possible [7], it provides inhomogeneous shared environment dependent on the position of a cell in the stream [2]. Actively actuated traps may offer better control over microenvironment and cross-contamination, but require the use of a complicated set of microfluidic valves and pumps that is limited by the number of connections and as such is not scalable to large numbers of cells ($>10^3$–10^4) [2], [4]. Droplet-based devices encapsulate cells in small volumes of water-in-oil emulsions [5] and provide room for combinatorial screening [8], [9] and sorting [9], [10]; although highly-controlled and efficient loading is possible [5], [11], and cell viability may be preserved over extended time [8], controlling individual droplets still requires significant manipulations [2]. In

all cases above, a high degree of control, efficiency and throughput, guided by computational optimization based on hydrodynamics simulations [7], is achievable; however, it comes at a cost of an overall complexity of the analysis and limited potential for retrieval of individual cells of interest. In contrast, arrays of microwells utilizing stochastic loading of cells from suspension have offered a straightforward way of tracing characteristics of large numbers of single cells [6], [12], [13]; just like arrays of passive traps, they simplify automated microscopy but also allow cell recovery and expansion into the possible number and types of assays [13], generally making them more modular than micro total analysis systems (μTAS) described above [2].

The most common choice of material for LoC devices has been poly(dimethylsiloxane) (PDMS). Its wide adoption in academic labs is based on a unique combination of properties [14]: ease of replication based on soft lithography, high optical transparency and low autofluorescence compared to common plastics, versatility in surface modifications and elasticity allowing it to conformally seal against hard surfaces and be actuated, permeability to gases, relative inertness and biocompatibility, along with a few others. Even with all these advantages, however, PDMS is not an ideal material for some applications [15]: its high permeability to small non-polar molecules and water vapor may severely affect measurements involving hydrophobic moieties and affect viability of cells sensitive to changes of osmolality in the media; its high elasticity precludes fabrication of microstructures with aspect ratios higher than 2:1 (e.g. tall posts) or lower than 0.2 (shallow channels or wells), and affects reliable registration for large-scale devices [16]. Finally, and perhaps most importantly, PDMS is not readily amenable to large-scale replication: while manual handling in an academic lab is straightforward, it takes a substantial time to cure the polymer (1–2h), and the overall process may leave residues on the mold. Industrial processes (such as injection molding), to the contrary, benefit from materials that can easily be processed and ejected in a matter of seconds, making large-scale production cost effective. There are alternatives to PDMS that may share some of its excellent properties but offer an improvement over others; one example is biocompatible thermoplastic cyclic olefin polymer

(COP) [17], as discussed in Chapter 2.

During initial development, any single-cell technology, along with associated materials and methods of fabrication, may be suboptimal or cater only to the needs of an academic lab. However, as we consider a wider adoption of these technologies and a greater impact in both scientific and clinical circles, we need to carefully evaluate and design each set of consumables and processes at each stage of their development. Steady improvements in these directions may make a substantial difference in how a technology is used, and bring about new revolutions in methodologies similar to the one that started with next-generation DNA sequencing.

1.2 Scope of thesis

In this thesis, we demonstrate two examples of single-cell technologies that exhibit some of the features described above. Particular focus is given to the design and development of *tools* that address certain aspects of single-cell analyses. We also demonstrate application of these technologies to several biological questions, although we don't aim to obtain substantial insights.

Chapter 2 covers the development of a new mass spectrometry-based technique to analyze tens of thousands of cells in a high-throughput fashion on a single chip. This method merges fluorescence cytometry with orthogonal label-free profiling of the lipid or metabolic content of each cell. We evaluate several choices of materials and approaches to chip fabrication suitable for interfacing with the mass spectrometric instrument. We also develop an analytical pipeline to efficiently process cells on the final device and demonstrate its application to the analysis of brain tumor samples.

Chapter 3 introduces an improvement over an existing platform for single-cell cytometry developed by our group. We design a new format of our arrays that improves their compatibility with a range of automated equipment and enables more efficient processing of a greater number of samples, while preserving viability and identity of each cell. We demonstrate its utility for enrichment, identification and recovery of rare circulating tumor cells (CTCs) and high-content immunophenotyping of small clinical samples.

Chapter 4 presents the conclusions of the thesis and lays out the ground for future work.

2. Small-molecule profiling of cells by MALDI MSI

2.1 Introduction

The World Health Organization (WHO) classifies over 125 types of brain tumors based on histopathological evaluation [18], assigning type, subtype and grade (I-IV) to each one of them. Gliomas, tumors of the tissue that support and protect neurons, account for 30% of them, with astrocytoma and oligodendroglioma being the most malignant forms, 70% grade III or higher. Glioblastoma (GBM) is astrocytoma grade IV, with a median survival of 12 to 15 months. Meningiomas account for another 34.7% of all brain tumors [19]. GBM is infamous for being one of the most heterogeneous tumors in existence, as defined by numerous phenotypic and genetic factors [20], [21]. Tumor sustainability and drug resistance are direct results of this heterogeneity, wherein tumor survives due to hyper-adaptive subpopulations. Identification of these tumors based on histopathology and magnetic resonance imaging (MRI) can be challenging, and decisions on surgical resection are in many cases too aggressive if the boundary between the tumor and the normal tissue is unclear [22]. This results in postoperative morbidity, i.e. undesired neurological deficits.

To help with identification and characterization of tumor heterogeneity, new modalities for tumor imaging are in dire need. More complete knowledge about the tumors could inform clinical decisions, and further enhance our understanding of tumor biology. Whereas conventional tools for resolving heterogeneity revolve around fluorescence microscopy at the proteomic and genomic levels, mass spectrometric techniques for identification and quantification of complex ($\gtrsim$100Da) molecules have also become available in the last two decades. Desorption electrospray ionization (DESI) mass spectrometry has recently been shown to accurately identify tumor type, grade and cellularity based on lipid imaging of tissue sections from stereotactic biopsies with a high degree of accuracy in near real time (i.e., during an operation) [19], [23]. Matrix-assisted laser desorption/ionization (MALDI) mass spectrometry imaging (MSI) has been

used for a proteomic-based prognosis in a similar context [24]. These advances demonstrate a clear clinical impact associated with such technologies.

While conventional methods rely on expensive probes (such as antibodies and DNA tags) that are specific to the molecules of interest, mass-spectrometric techniques mentioned above allow for direct imaging of small and large molecules without the need for any labeling. In case of small molecules (such as lipids and metabolites), highly specific probes may not even exist. Additionally, this allows us to work in "discovery mode", where mass spectrum signals can be analyzed with little or no a priori knowledge of what particular molecules to look for, which would not be possible with methods that rely on labeling of target analytes. Little or no sample preparation also reduces the time and effort required for MSI compared to probe-based analyses.

At the same time, the number of parameters that could conceivably be simultaneously accessed through MSI-based tests is measured in the hundreds, which is vastly greater than for fluorescent or isotopic probes. While some inconvenience and ambiguity in interpretation of the spectra may exist due to inaccuracy of the instruments and complex fragmentation patterns of the molecules, steady improvements in these directions will allow for even better specificity and increased dimensionality in the future.

As mentioned above, imaging mass spectrometry has mainly concerned itself with the analysis of tissue sections, but not at the single-cell level. There are multiple factors that account for this. First, the maximum spatial resolution of current instruments is limited by the diameter of the scanning probes, which is ca. 125 um in case of DESI and ca. 20 um for MALDI. While this limit could be somewhat improved through the use of "oversampling" [25], i.e. spatially overlapping consecutive desorption events, it still hardly approaches the size of individual cells and is not reliable enough to resolve neighboring cells. We can reasonably hope that future improvements in instrumentation will allow us to bridge this gap. However, methods relying on spatial isolation of individual cells are currently required. MALDI also seems to be a clear winner in terms of resolution, compared to other desorption techniques.

Second, the sensitivity of the instruments is limited by the amount of material needed to build a peak, i.e. the number of molecules counted by the detector. While the limits of detection achievable by MALDI have been reported to be in the attomole (and potentially down to low zeptomole) range [26], this still amounts to a detection threshold of ~10^5 molecules and is not readily available for most substances and instruments. Realistically, only femtomole amounts of material are detected in a typical setup, limiting us to the detection of the most abundant molecules in native samples or upconcentrated analytes extracted from a tissue after chromatography.

The instruments for MSI have certainly progressed over the years, providing incremental improvements over mass sensitivities, as well as better spatial and mass resolutions. However, because of the cost, time and technical expertise required to upgrade the instrumentation, it has not been always under direct researcher's control to improve hardware characteristics. To the contrary, sample processing protocols could easily be changed from their standardized counterparts. An overarching topic in the literature on increasing sensitivity based on sample preparation is minimization of spreading of analyzed molecules, which up-concentrates them in more confined areas. Various methods to prevent lateral diffusion have been proposed.

As suggested by its name, MALDI uses a special coating ("matrix") that incorporates analyzed molecules, and absorbs the energy of laser irradiation to vaporize together with these molecules, ionizing them in the process (**Figure 1**). One approach to sample preparation involves fixation of the tissues or cells with a chemical treatment either before or during the matrix deposition [27], [28]. Different fixatives allow for extraction of lipids and salt adducts from the sample, while exposing internal cellular structures for co-crystallization with the matrix, as well as dehydrating the sample to minimize diffusion. Alternatively, some solvents are compatible with lipids and can in fact enhance their signal by cross-linking peptides and proteins [28], [29].

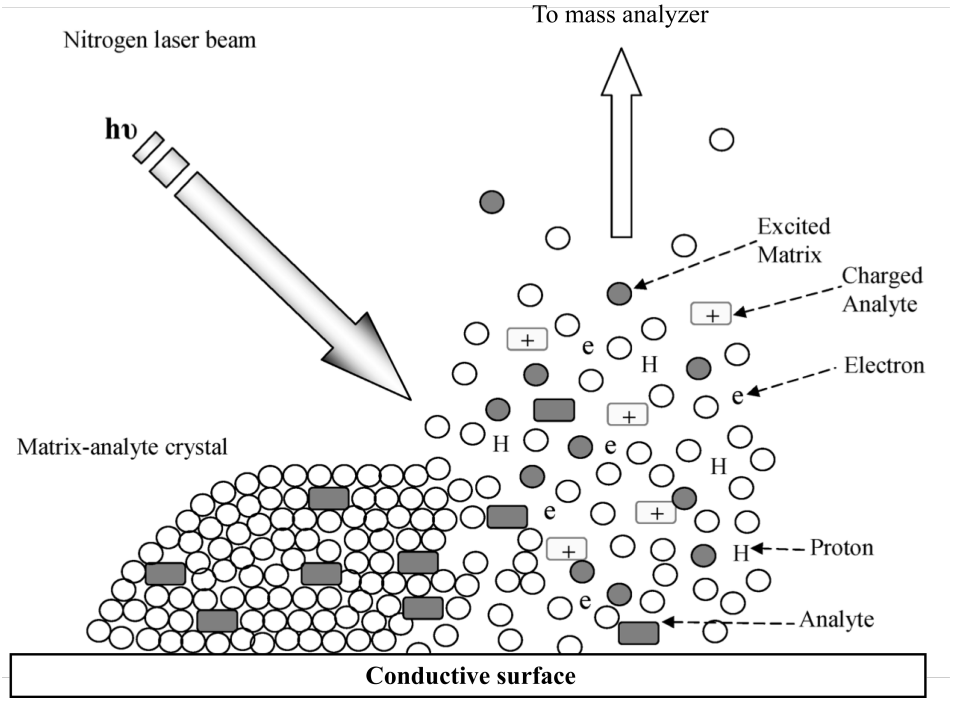

Figure 1. Ionization process in a MALDI time-of-flight (TOF) instrument. The matrix-analyte crystal is bombarded with a UV laser beam that excites the matrix, which, in turn, transfers the energy to the analytes. This results in the ionization and desorption of the analytes, mainly as singly charged species. The remaining charge dissipates via a conductive substrate. Adapted from [30]

Another important aspect is the method of deposition of the matrix. The main focus is to prepare homogeneous matrix crystals that optimally incorporate analytes of interest, while also minimizing their lateral spread. Various deposition techniques have been developed to address these points (**Figure 2**). Among these are nebulized spray coating through a nozzle [31], commercially realized in the Bruker ImagePrep instruments; electrospray [32] and automated piezoelectric inkjet-type deposition [33], [34]; matrix microinjection [35]; sublimation with recrystallization [36], [37]; or combinations of these [38]. A comparison of them can be found in [35] and [39]. Important aspects of all these techniques are their cost-effectiveness; time and reagent consumption; quality, size and homogeneity of the crystals and analyte incorporation; and potentially some other factors. In the context of high-throughput processing and spatial resolution, matrix sublimation with recrystallization appears to be the most effective thus far.

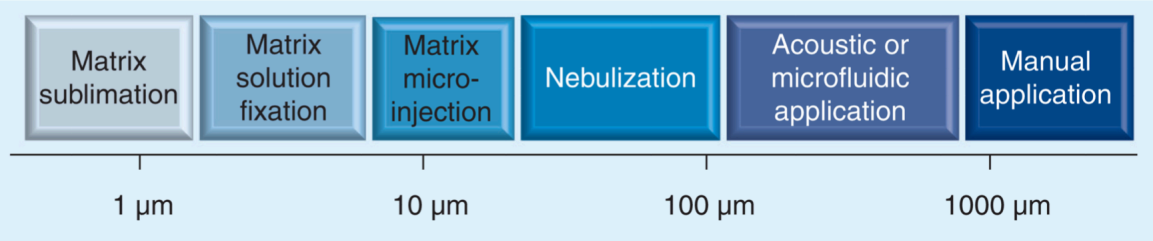

Figure 2. Spatial resolution of matrix deposition methods. Reprinted from [39]

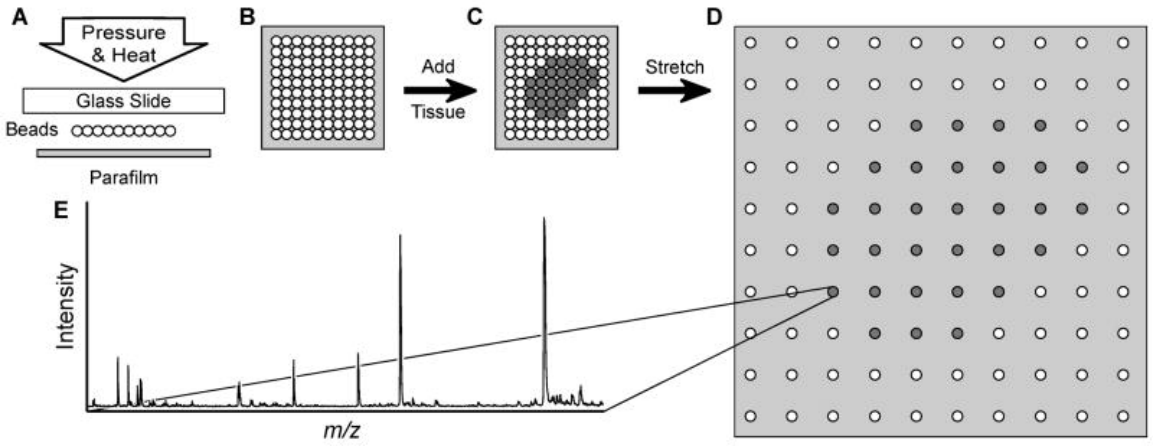

Figure 3. Schematic of the massively parallel sample preparation using the stretched sample method. **(A, B)** Pressure and heat are used to form a layer of glass beads on a Parafilm M membrane surface. **(C)** A thin tissue slice is placed onto the glass bead layer. **(D)** The Parafilm M membrane is manually stretched. As a result, the tissue slice is fragmented into thousands of spatially isolated pieces. **(E)** After MALDI matrix application, individual pieces of tissue may then be investigated with MALDI MS. Reprinted from [40].

Finally, spatial separation of analyzed spots could ultimately prevent sample cross-contamination and lateral spread. A number of techniques have been used in this regard, starting with robotic spotting or ink-jet printing as noted above. However, many of such approaches are serial in nature, not allowing for the highest throughput that could be achieved with parallel methods. More recently, a stretched tissue approach has been proposed to address this problem (**Figure 3**) and demonstrated the feasibility of tissue analysis at a single-cell scale: an array of glass beads is embedded in parafilm, and a tissue slice is mounted onto the beads and then uniformly stretched to produce single-cell sized pieces separated by hydrophobic regions, which prevent further analyte migration. This approach has the same effect as dried-droplet preparation

of samples on the commercial AnchorChip^{TM} [41].

The idea of compartmentalization drove the bulk of research on increasing sensitivity based on sample preparation. Indeed, one of the first methods to detect attomole amounts of analytes proposed the use of picoliter pyramidal vials etched in Si [42]. In these vials, solvent evaporates in a few seconds and leads to homogeneous micron-scale crystals at the edges of the pyramids. Interestingly, the authors also concluded that *"the potential of transferring **single cells** to the picolitre vials, followed by the addition of the matrix solution, gives the possibilities of following cell-specific processing of proteins, post-translational modifications and peptide sorting and targeting to different intracellular sites"*. To the best of our knowledge, however, they never followed up on this promise, which we attribute to the lack of the tools for high-throughput imaging and automation available at the time, as well as an overall sensitivity of the instruments.

As described in Chapter 1, the use of microwells to compartmentalize cells is not novel. Recent advancements in soft lithography allowed for a wide-spread use of poly(dimethylsiloxane) (PDMS) stamps to trap and image single cells in the microwells of a suitable size [6]. In the context of our laboratory, these devices have been successfully used to study protein secretion from heterogeneous cell populations, whereby the wells are sealed against a glass slide to provide a local microenvironment for each cell, up-concentrate secreted factors and capture them on the surface of the slide [13], [43] (**Figure 4**). Microwell arrays are amenable to automated imaging and image processing, simplifying spatial localization of the isolated cells. Yet, to the best of our knowledge there are currently no high-throughput platforms based on microwells that would directly couple fluorescence-based assays to MALDI MSI to combine the advantages of both. Here we present the first example of such a system.

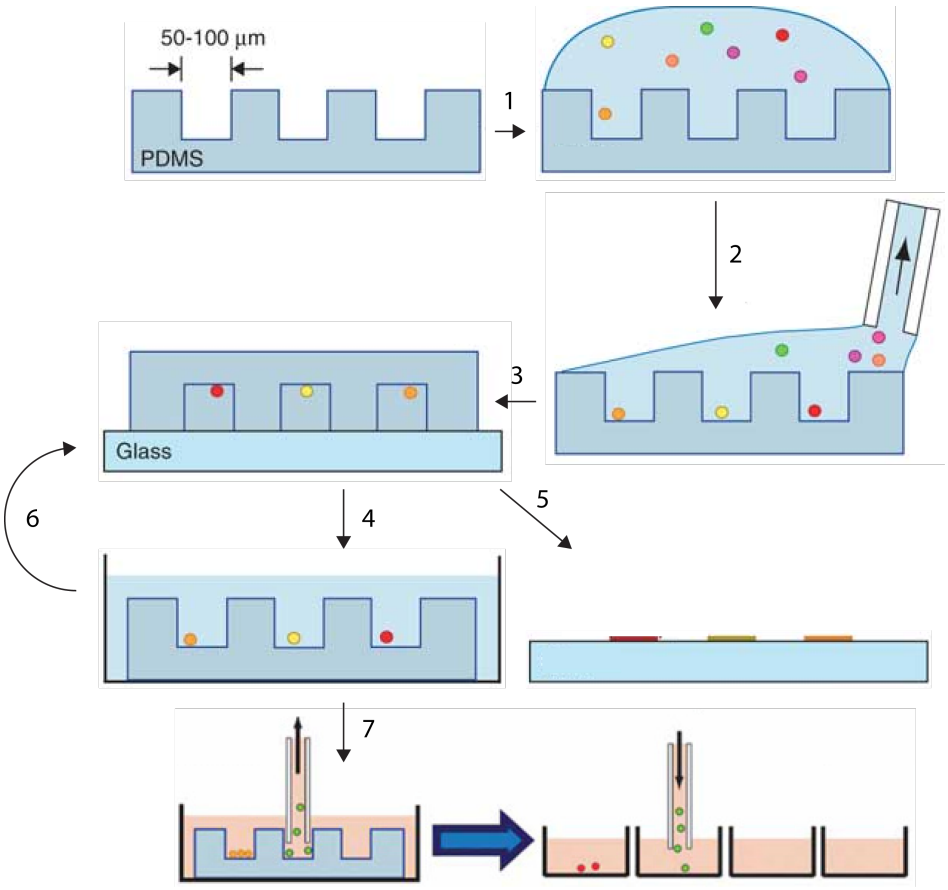

Figure 4. Schematic diagram of the processes involved in microengraving. (1) A suspension of cells is deposited onto an array of microwells fabricated by soft lithography. (2) The cells are allowed to settle into the wells and then the excess medium is removed by aspiration. (3) The dewetted array is placed in contact with a pretreated solid support, compressed lightly and incubated for 2–4 h. (4) The microwells are removed from the solid support and placed in a reservoir of medium. (5) In parallel, the secreted factors captured on the solid support can be quantified in a microarray scanner. (6) Printing for secreted factors can be done repeatedly to different slides. (7) The cells of interest can be retrieved by micromanipulation and transferred to a 96-well plate for downstream analysis. Adapted from [13], [43].

2.2 Results

Microwell devices currently used in our laboratory cannot be directly imaged in a MALDI time-of-flight (TOF) instrument. The latter requires conductive substrates such as indium tin oxide (ITO) coated glass slides, or metal plates. TOF mass analyzers measure the time travelled by ions over a spatially fixed electric potential difference and thus depend on the initial velocities/kinetic energies of the ions [44]. If the substrate is non-conductive, electrons resulting

from ionization do not dissipate, accumulating charge locally and distorting the accelerating potential, resulting in reduced mass resolution and accuracy [45], [46]. Although this effect can be reduced in ion-trap mass analyzers such as FTICR because they measure cyclotron frequency $\omega = qB/m$ that only depends on ion charge/mass ratio and the magnetic field, we expect that charging effects may still negatively impact overall quality of the signal and complicate calibration [46], [47].

Here we developed two approaches to address this problem. In the first approach, we can still use PDMS devices without or with only a minor modification of the established protocols. We would then seal the array with an ITO-coated slide, and transfer the cells from the microwells to the slide. This approach could allow us to conduct cytometry and serially print for secreted proteins, and only perform the destructive step of MALDI on cells of interest in the end.

In the second approach, we make microwell devices conductive by themselves. This allows us to perform all the steps on the same chip, precluding potential loss of cells and their patterns in the process of transfer. We will also explore several materials suitable for making devices conductive.

2.2.1 Cell transfer

We first sought to transfer cells from existing PDMS-based microwell arrays to an ITO slide. High-quality flat glass substrates commercially coated with ITO are ideally suited for microscopic imaging due to over 90% transmission of ITO in the visible range [48] and its high conductivity on the order of 10^4 S/cm [49]. However, we need to ensure that the cells are transferred efficiently, and that we could relate their locations on the slide to their prior locations in a microwell array.

For the process of transfer, we needed a high shear force that would act on cells to drive them out of the wells onto the slide. In the regular process of microengraving, a PDMS stamp and a glass slide are conformally sealed together using a metal clamp with a tightening screw (**Figure**

5). Several other sealing configurations were tested when the microengraving process was developed, but the metal clamp gave the best results when "printing" for secreted factors. As such, it was natural to repeat this process for cell transfer as well.

Figure 5. Agilent Microarray Hybridization Chamber

To confirm cell transfer, we would then unseal the stamp and the slide and observe them separately under a microscope. The unsealing process introduces additional shear forces that could destroy the pattern if we are not careful enough. To address this, we placed the "sandwiched" stamp and slide in phosphate-buffered saline (PBS) and either let the slide float away, or gently pry opened the assembly with tweezers.

To apply the forces for cell transfer, we first tried to rotate the clamp such that an ITO slide sits at the bottom, and tap it against a hard surface. Unfortunately, the forces provided in this way were insufficient, as most cells stayed in the wells, and the slide remained essentially clean.

We then applied a more universal way to pull down the cells, used in most wet laboratories, – centrifuging. We placed the metal clamps in prototyped Styrofoam holders, and rotated them at a high r.p.m. This process finally gave us positive results, although the rate of transfer was still not sufficient.

To facilitate the transfer further, we sought to prevent cells from holding onto the stamp. This could be accomplished with a "slippery" coating applied to PDMS *before* we loaded cells on it. In a regular microengraving process, we coat the stamps with bovine serum albumin (BSA) to prevent their surface from adsorbing secreted proteins. Although this process works well for the

proteins, it was insufficient to prevent cell attachment in our tests. A more robust biocompatible coating that is ubiquitously used to passive surfaces is polyethylene glycol (PEG). To attach the nonpolar PEG molecules to the surface of the stamp, we used PEG-g-PLL, a graft copolymer of PEG with poly-L-lysine. PLL is positively charged at physiological pH, and will adsorb to any negatively charged surface. PDMS is normally nonpolar, but can be temporarily oxidized with a plasma discharge [50].

Although coating of PDMS with PEG provided a more reliable cell transfer and we could distinctly observe rectangular arrays of cells (**Figure 6**A), we still needed a means to trace the location of each cell after its transfer from the stamp to the slide. In the microengraving process, we face a similar problem of identifying the locations of secreted proteins in the array; we normally solve this by spiking the printing media with a "background" molecule, which would be present in every well and as such would provide an "imprint" of an entire array on the slide. While this approach could certainly work to identify cell locations after cell transfer, MALDI imaging is notoriously sensitive to any background signal that could dominate the spectra and make the analysis infeasible. One solution to this problem would be to "invert" the background, whereby the molecule to be used as background would be present everywhere but the locations of the wells (and cells). In fact, PDMS has been extensively used in micro-contact printing (μCP), which is a soft-lithographic technique to "print" molecules from the raised features of the stamp to the substrate. While μCP has initially been developed to produce self-assembled monolayers of alkanethiols on gold-coated slides, it has since been shown to work for many other combinations of "inks" and substrates [51]. We decided to print fluorescently labeled BSA onto PLL-coated ITO slides (that is, to use essentially the same materials as in the normal microengraving process). While μCP in this case proved successful over small areas (**Figure 6**B), large-scale repeatability of the printing was inconsistent (with huge "pockets" of surface not transferred at all), which we attribute to inhomogeneity of the stamp and applied pressure across large areas, as well as presence of liquid in some areas between the stamp and the slide. Overall, μCP could still

be used for partial registration of the slide when absolutely needed.

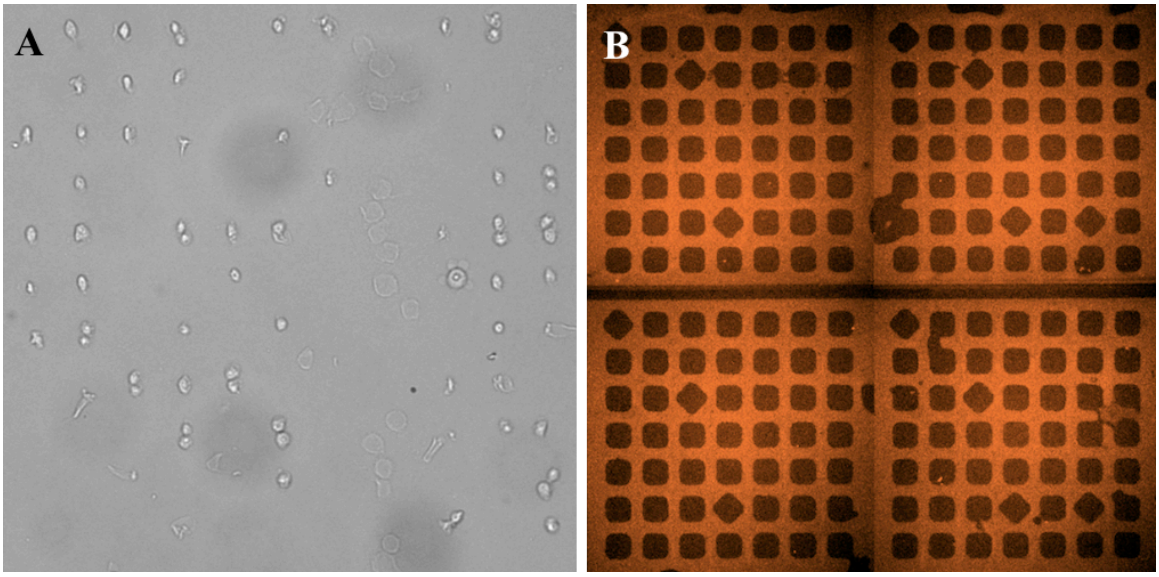

Figure 6. (A) Cells transferred from a PEG-g-PLL-coated PDMS stamp with 30 um well size to a PLL-coated glass slide in a metal clamp centrifuged at 1000 rpm (~200g) for 5 min. (**B)** Rhodamine-conjugated 5mg/mL BSA contact printed from PDMS with 50 um wells to a PLL-coated ITO slide. PLL is a 0.01% w/v stock. Both images were taken on Zeiss AxioObserver Z1 at 10x with 800 um field of view corresponding to one block of wells. 4 adjacent images are stitched and their contrast enhanced in B.

As noted above, BSA proved to be less effective at preventing adhesion of cells to the stamp, while providing only subpar registration pattern. A better alternative, PEG could not be printed to the slide; but even with PEG the cell transfer rate was not as high as desired (tentatively, <50%). These problems led us to look for a more direct approach to sample cells with MALDI.

2.2.2 Plastic devices

The microwell devices could be directly used in a MALDI instrument if we modified them in certain ways. Since PDMS is a dielectric, we sought to create a conductive film on top of the wells to match that of the commercial ITO-coated slides (sheet resistance 100 Ohm/sq or higher). PDMS had to also be substituted for a hard plastic that would provide enough rigidity as a substrate for film growth and mechanical handling (thin films created on a soft layer would

easily crack).

In recent years, cyclic olefin polymers (COPs) have gained popularity as a substitute for PDMS in lab on-a-chip applications [17]. Unlike the latter, COPs are thermoplastics, suitable for high-volume production using injection molding. They also provide superior optical properties, with the highest level of transmission (~92%) from near-UV to near-IR range among other common plastics (PS, PMMA etc.), and a low level of auto-fluorescence. COPs, similarly to polypropylene (PP), are also chemically inert and biocompatible. We prototyped COP chips using soft embossing, a technique of replication of microscopic features whereby an elastomeric stamp is used as an intermediary mold for replication [52] (**Figure 7**A); the initial master remained the same as for our regular PDMS stamps.

To facilitate imaging cytometry, we decided to keep the devices transparent. A thin layer of ITO (~120 nm) or gold (~20 nm, with Ti for adhesion) could be a suitable material for a transparent conductive film. Common processes for thin film deposition that are compatible with low-temperature processing of the thermoplastics include sputtering and e-beam evaporation. Sputtering provides improved sidewall coverage, as required to form a continuous film on top of the chips as an electrode for MALDI; sputtering also preserves stoichiometry of compound materials, such as ITO (nominally 90% In_2O_3, 10% SnO_2 wt.).

After fluorescence cytometry, we coated the chip with a suitable matrix using Bruker ImagePrep system for matrix nebulization, which is normally used for MALDI imaging of tissue section samples (a sublimation apparatus was not available at the time). We then attempted to image rectangular areas of the chip in a MALDI instrument to get a sense of the spectra. However, we were unable to acquire a high-quality signal. The molecular image of the wells appeared dark (no signal) (**Figure 7**B), and the secondary electron images of the wells in a scanning electron microscope (SEM) demonstrated a charging effect at the walls of the wells (**Figure 7**C). These results suggested that the sputtering procedure might not have formed a continuous conductive layer at the sidewalls, leading to excessive charge buildup inside the wells

during these observations (however, we have not confirmed this with a cross-sectional SEM, since we decided to abandon the entire approach, as described below). This charge would alter initial velocities of the ions in a time-of-flight MALDI instrument and prevent us from getting a suitable signal. Another possible reason for the absence of MALDI signal is the occlusion of the laser beam by the vertical profile of the walls, as the laser is directed at the surface of the chip at an oblique angle.

MALDI signal was also dominated by peaks reminiscent of the underlying polymer (**Figure 7**E), suggesting that the laser beam could have ablated the polymer through the film. Indeed, typical laser fluence in MALDI instruments is 10–100 mJ/cm^2 or higher [53], nearing threshold fluence for the ablation of most polymers [54]. The film should be relatively transparent to the wavelengths of the laser (337nm and 355nm): according to the tabulated values of the absorption coefficient, $\alpha \sim 10^4$ cm^{-1} for ITO [48] or $\alpha \sim 6x10^5$ cm^{-1} for gold [55], which for the thicknesses d ~ 120nm (ITO) or d ~ 20nm (gold) translate to an exponential decay of 0.9 (ITO) or 0.3 (gold). Excessive charging of the ablated areas in SEM also suggested that the conductive layer might have been fully or partially removed (**Figure 7**D).

Finally, the polymer contaminated the vacuum in the MALDI instrument, which we attributed to its ablation mentioned above, as well as possible outgassing of the chip in the vacuum. Subsequently, the instrument ceased to detect any signal (even for unrelated experiments), and had to be cleaned extensively before it could be used again.

Although we could design a quarter-wavelength stack of films to be reflective to the laser, or simply increase the thickness of the film (>100nm of gold, which demonstrated similar results), this would complicate the fabrication procedure without necessarily improving the performance of the chip, while also making it optically opaque for imaging cytometry. As such, we decided to abandon this approach and use a more robust material for our devices.

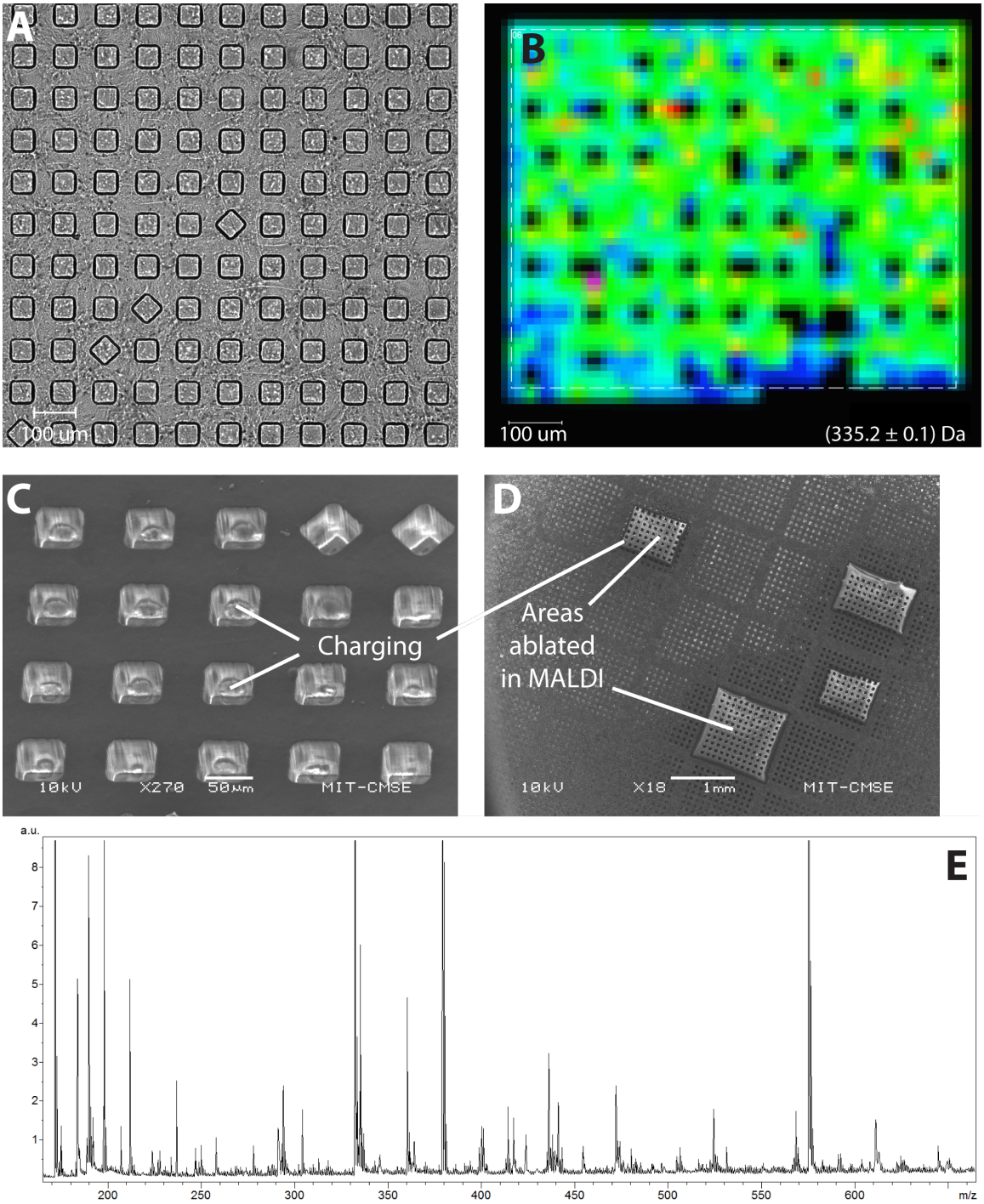

Figure 7. MALDI imaging of a plastic chip coated with gold. **(A)** Transmitted light image of a block of wells soft-embossed in COP. **(B)** Molecular ion image of a block. **(C)** Secondary electron (SE) image of the wells in SEM. **(D)** SE image of the ablated blocks in SEM. **(E)** MALDI spectrum from top of the wells.

2.2.3 Si chips

While thermoplastics would be desirable materials for the mass-production of our devices, their stability was not sufficient for MALDI experiments, as described above. The primary material used in the fabrication of microstructures, however, is silicon. It is directly compatible with well-established and reproducible microfabrication procedures used in cleanrooms, providing the means for a high-volume production. It has high thermal and vacuum stability, preventing any contamination due to melting or outgassing in a MALDI instrument. Si wafers provide an extremely flat surface, and the rigidity of silicon ensures strictly rectangular arrangement of the wells, without long-distance warping and pattern distortions characteristic to polymers. Finally, the crystal structure of Si allows for anisotropic etching of microfeatures with slanted walls [56], which could address the problem of occlusion of the laser beam mentioned above. Additionally, silicon could act as a conductive material on its own, precluding the need for any conductive coatings.

The basic workflow for successful on-chip cytometry using Si chips is outlined in **Figure 8**. The process starts with the design of a suitable mask that is then used to photolithographically define arrays of the wells and registration marks on Si wafers during the fabrication procedure. After the devices are fabricated, we prepare and load cells on a chip. We then image the array in an automated fluorescence microscope. Acquired images need to be processed to identify the locations of wells with the cells. To prepare the chip for MALDI MSI, we deposit the matrix using a custom sublimation protocol. The MALDI imaging software requires a global "map" of an entire chip for navigation; the global positions of the wells of interest need to be defined with respect to the corner points on this map. After this registration is done, we proceed with an automated acquisition of MALDI spectra across the array. Finally, we analyze the spectra to define peaks of interest and relate them back to the fluorescent signal.

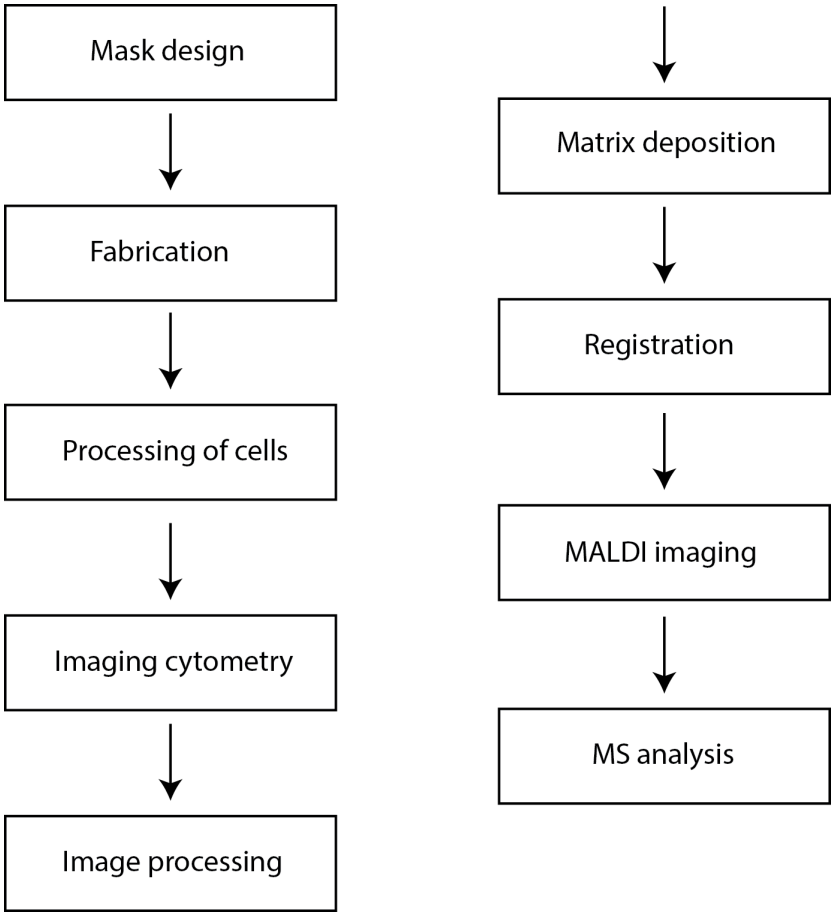

Figure 8. Workflow for on-chip cytometry with Si chips.

To design masks, we created custom software that generates CAD files from user-defined parameters and is tailored to the arrangement of features in our arrays. We arranged features into blocks, with each block corresponding to one field of view of the camera on the microscope (**Figure 9**). To be able to later create a "map" of the chip by stitching the images together, we engineered an overlapping space spanned by the camera between neighboring blocks. We also introduced numbers labeling the positions of blocks on the chip to facilitate visual navigation in the MALDI instrument, as well as to help with the stitching. Since the undercut resulting from anisotropic etching of <100> Si is minimal only when the features' edges are either parallel or orthogonal to the wafer flat, the digits had to be broken up into little squares instead of remaining solid pieces. Due to the minimal undercut, the features corresponding to the wells could be placed

as close as 10um to each other if we wanted to analyze more cells and reduce the "dead" area of the chip. We also engineered a border surrounding the chip, such that when placed in the instrument, the wells would be raised, with their bottom corresponding to the reference plane expected by the instrument, as there was some concern that being out of plane would affect the measurements. For identification of the chips and their orientation, we placed a side caption detailing the geometric parameters of the chip, to be viewed with a naked eye. Finally, we added calibration areas and registration marks at the edges of the chip, although we have not used them in the final protocol. Since we had multiple chips per wafer area, we also drew the guides to cut out individual chips with a die saw.

For the fabrication of chips, we adopted a standard process used by the MEMS industry to produce cantilevers using anisotropic etching of Si (**Figure 10**). Briefly, we used low-pressure chemical vapor deposition (LPCVD) to deposit low-stress silicon nitride that would act as a masking layer during anisotropic etching. We then used photolithography to translate the features from our mask to this substrate. The photoresist pattern served as a temporary mask when we plasma-etched the silicon nitride to reveal the underlying Si. We then stripped photoresist with piranha solution and etched the silicon with a heated solution of potassium hydroxide (KOH) for a predetermined amount of time. Finally, we stripped the remaining nitride in hot phosphoric acid. Additionally, we used e-beam evaporation to deposit a thin layer of gold that served as an electrode on top of Si, as bare Si normally doesn't provide a good Ohmic contact because of the build-up of the depletion layer and native oxide (see Discussion on how to overcome this issue). **Figure 11** illustrates the final look of the wells in a scanning electron microscope (SEM) and an overview of an entire chip in visible light.

The protocol for processing of cells was developed using cultured cell lines. Before loading cells into the wells, we placed the chip in a plasma cleaner to promote removal of organic residues and make the surface more hydrophilic. The cells were stained and re-suspended in PBS to reduce the amount of background signal coming from the culture media or blood; cell

concentration was adjusted such that the total number of loaded cells would match several times the number of wells on the chip, to ensure efficient distribution of cells across the wells. We spread the solution of cells across the chip and, after a short incubation, washed out the excess by gently dispensing PBS from the short edges of the tilted chip; loaded cells remained trapped in the wells. Unfortunately, we could not observe the process of loading in transmitted light (as done regularly for the PDMS stamps), because Si is not transparent. Since we used an inverted setup for fluorescence microscopy, we also had to fix the cells to prevent them from falling when imaging face down; fixing might also help with extraction of small molecule analytes for MALDI imaging, as mentioned in the Introduction.

Fluorescence imaging was performed in an automated fashion using a pre-determined list of positions corresponding to locations of the blocks on the chip. We defined support points by focusing at the bottom of the wells for several locations in the array, and relied on spline interpolation of these points for all the positions in the list. To define the locations of the wells for subsequent image analysis, we had to modify our microscope setup to obtain bright-field (non-fluorescent) images of the blocks; we used a wide-band dichroic mirror to pass the excitation light (reflected from the sample) to the camera, and adjusted its intensity with a neutral density filter. Finally, we adjusted the magnification of the microscope to considerably reduce the amount of time spent on imaging, with minimal loss in resolution; this was possible because the camera had a high pixel count and low pixel size, and high resolution is not required for our purposes.

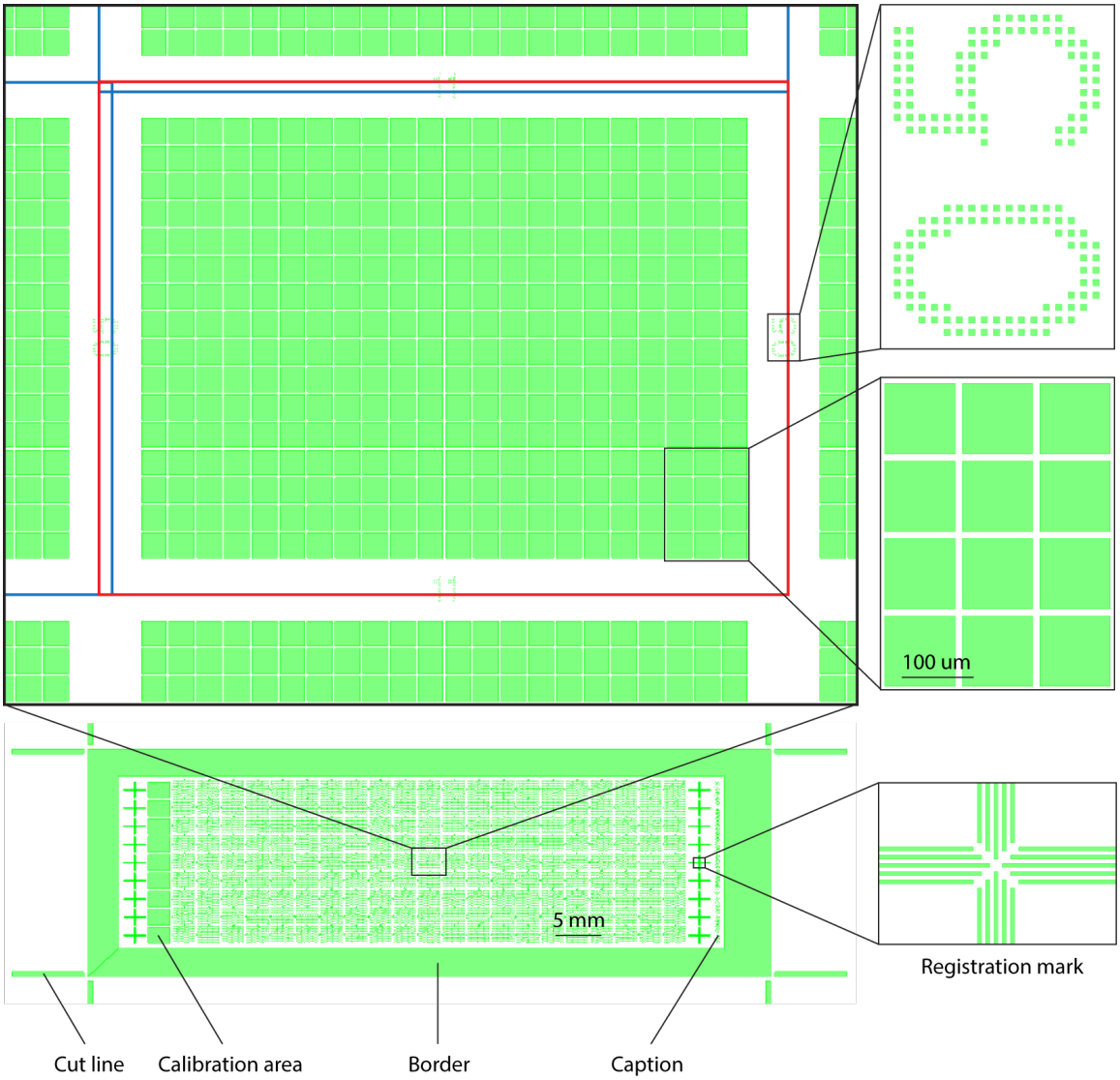

Figure 9. Design of the mask for fabrication of Si chips. Red rectangle delineates one field of view of the camera. Blue lines illustrate built-in overlap between these. Other features are explained in the text.

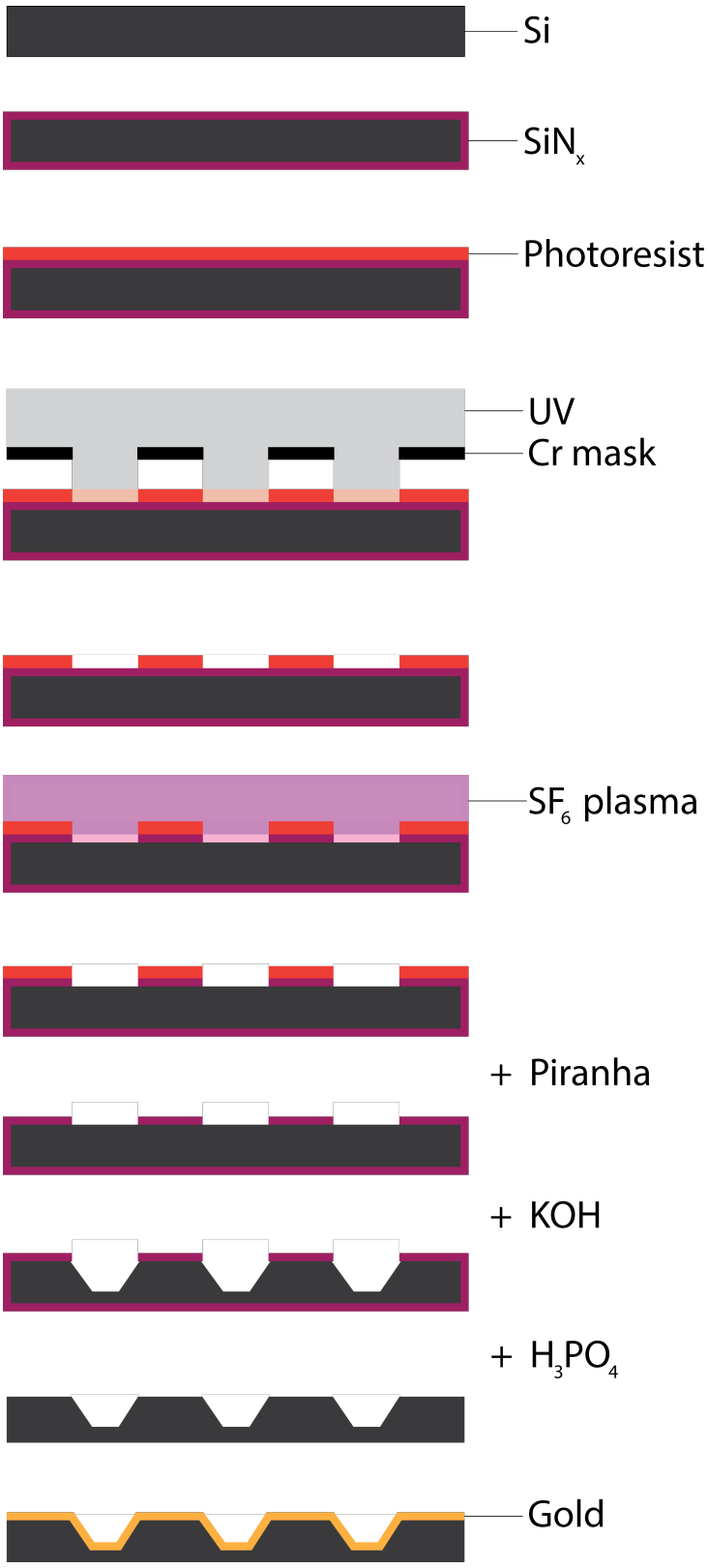

Figure 10. Fabrication of Si chips.

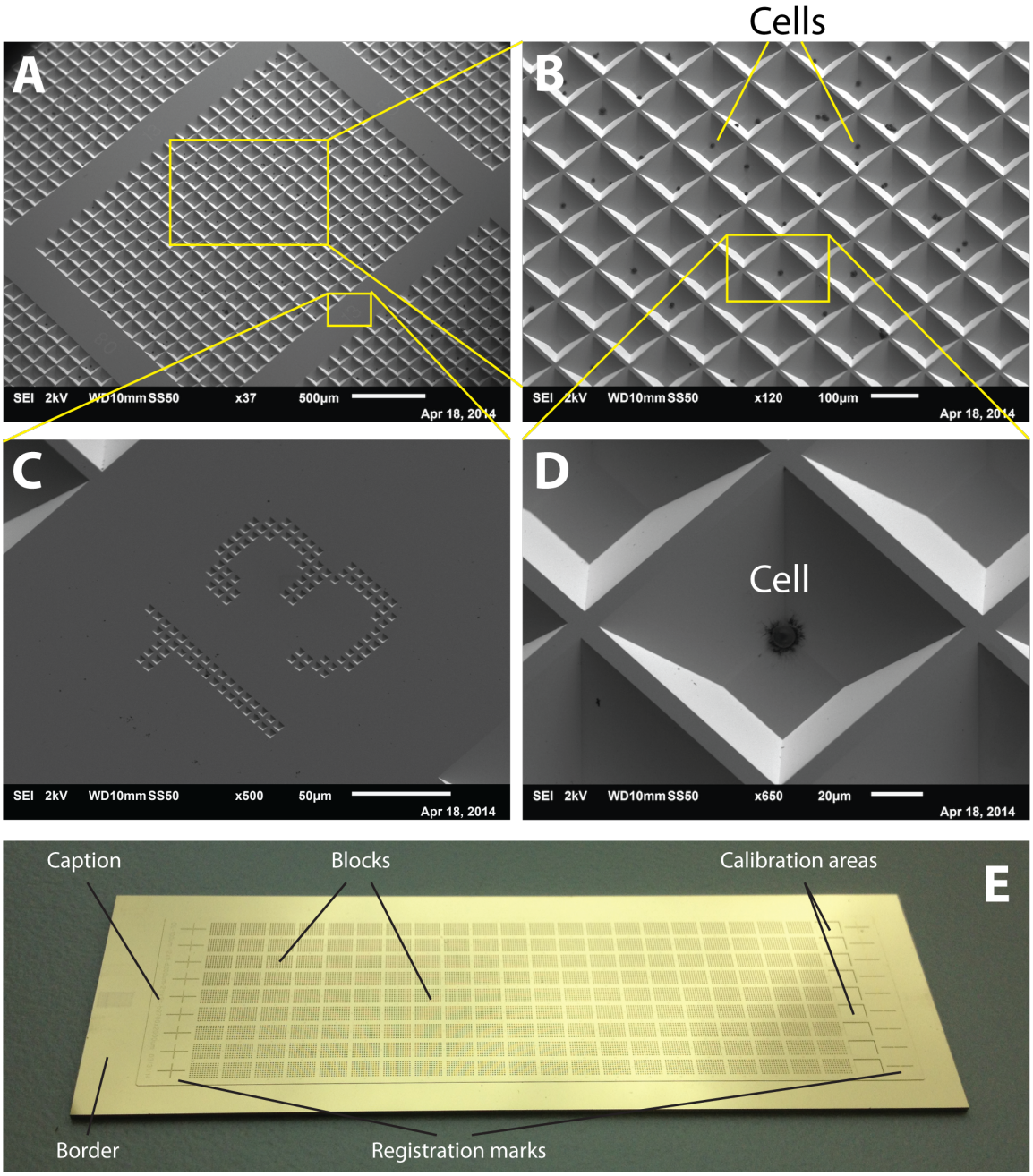

Figure 11. Fabricated Si chip. **(A)** Overview of a block of wells in SEM. **(B)** Close-up on multiple wells; black dots are cells settled in the wells. **(C)** A column number labeling position of the block on the chip. **(D)** A single well harboring a cell. **(E)** Overview of a finished chip in visible light.

Images of individual blocks were subsequently processed with a version of in-house automated image analysis software (Enumerator), modified to correctly detect pyramidal wells. Unfortunately, slanted walls of the wells were highly reflective, producing mirror images of each cell in the 4 walls of a well (**Figure 12**). These images were falsely identified as cells and prevented us from accurately counting the number of cells in each well. However, the mirror images had a specific pattern (forming a "cross" around each cell), which could be used to deduce the real locations of the cells if sub-well localization was required.

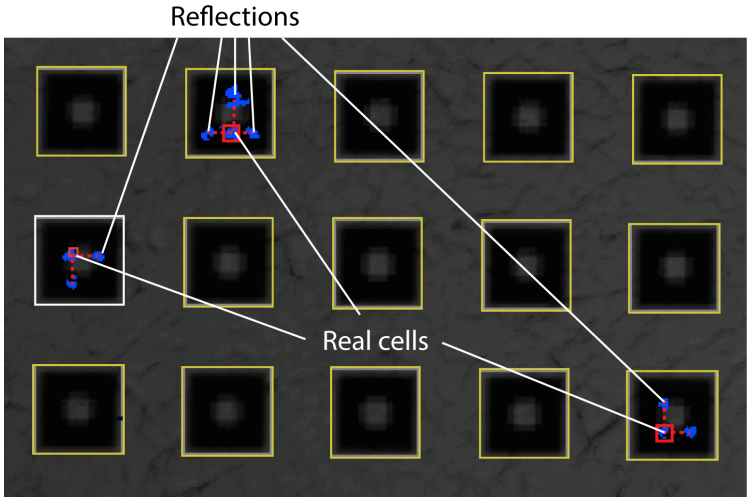

Figure 12. Part of an image analyzed by Enumerator.

To prepare the chip for molecular imaging in a MALDI instrument, we needed to deposit a matrix layer on top of the cells. As described in the Introduction, one of the methods of matrix deposition most suitable to our analysis is sublimation with re-crystallization. A custom sublimation apparatus and an optimized procedure were created to ensure a homogeneous layer of matrix, as described in Methods. We also re-crystallized this layer in a solvent-humidified chamber to partially incorporate the analytes of interest (i.e. phospholipids) into the matrix crystals.

For registration in the MALDI instrument's control software (flexImaging), a single

composite image of an entire chip is required. We employed a stitching plugin from ImageJ in a custom script to piece together the images of individual blocks (provided with pre-engineered overlap area and numbering) with sub-pixel accuracy. Along with excellent dimensional stability of Si, this allowed us to register wells with high precision, potentially suitable even for sub-well navigation.

To generate a list of positions to be acquired by MALDI, we exported an XML file with calibration information from flexImaging, and parsed it using a custom Python script to add the list of wells with cells as defined by Enumerator, along with a randomized list of empty wells used for control. An example map of the chip with added positions is shown in **Figure 13**, and the procedure for acquisition of MALDI signal is described in Methods.

As an initial test of the experimental workflow, we compared the detection of phospholipid signal in MALDI to the detection of fluorescent signal as the gold standard. Mouse fibroblast cells expressing enhanced green fluorescent protein (eGFP) were loaded onto an array, and wells containing cells were identified through fluorescent imaging. Occupied wells, along with a random sample of empty wells, were then subjected to MALDI analysis. Receiver operating characteristic (ROC) curves (**Figure 14**) suggest a high degree of correlation between fluorescent and MALDI signal for many m/z values that were handpicked by a trained specialist from the MALDI spectra.

We next determined whether single cell MALDI spectra were capable of identifying unique cell populations. We initially compared phospholipid profiles of two distinct cell lines processed on separate chips (**Figure 15**). Principle component analysis (PCA) successfully segregated the two cell lines (**Figure 15**C). The analysis also revealed characteristic peaks that could serve as cellular signatures (**Figure 15**D). We then mixed these two populations on a single chip and confirmed that cell lines could indeed be split from each other based on such signatures (**Figure 16**).

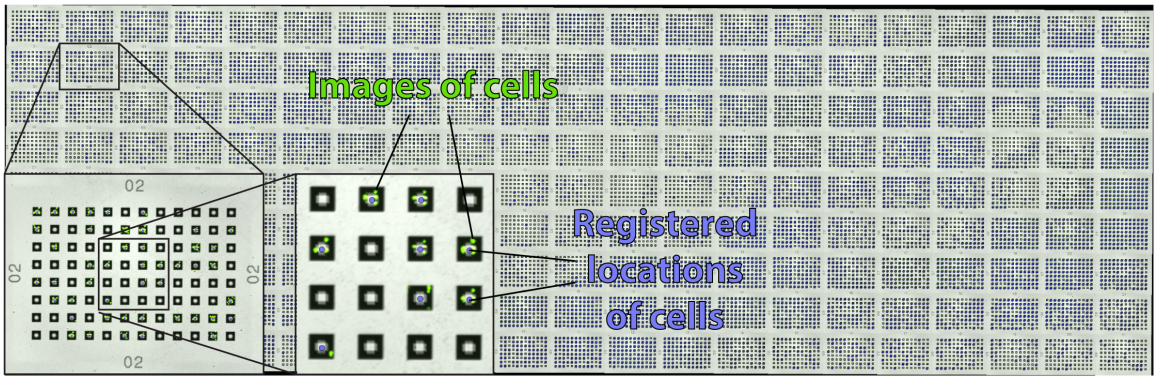

Figure 13. Map of a Si chip with calculated positions of cells for acquisition in MALDI (blue dots).

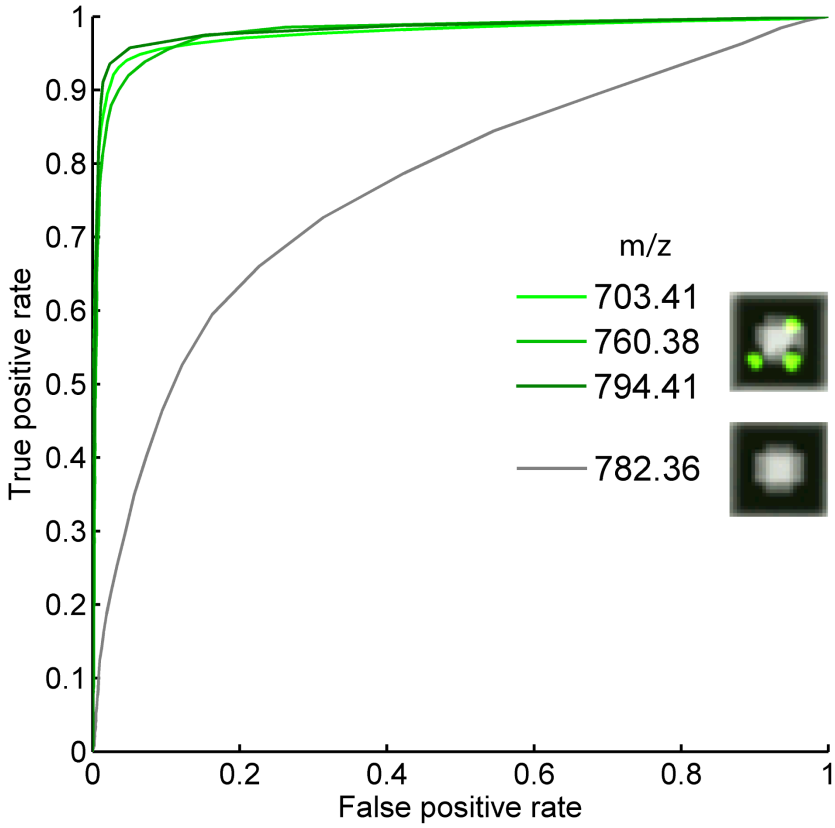

Figure 14. Receiver operating characteristic for prediction of wells with MALDI signal based on fluorescence. Green curves correspond to wells with cells, gray – to empty wells.

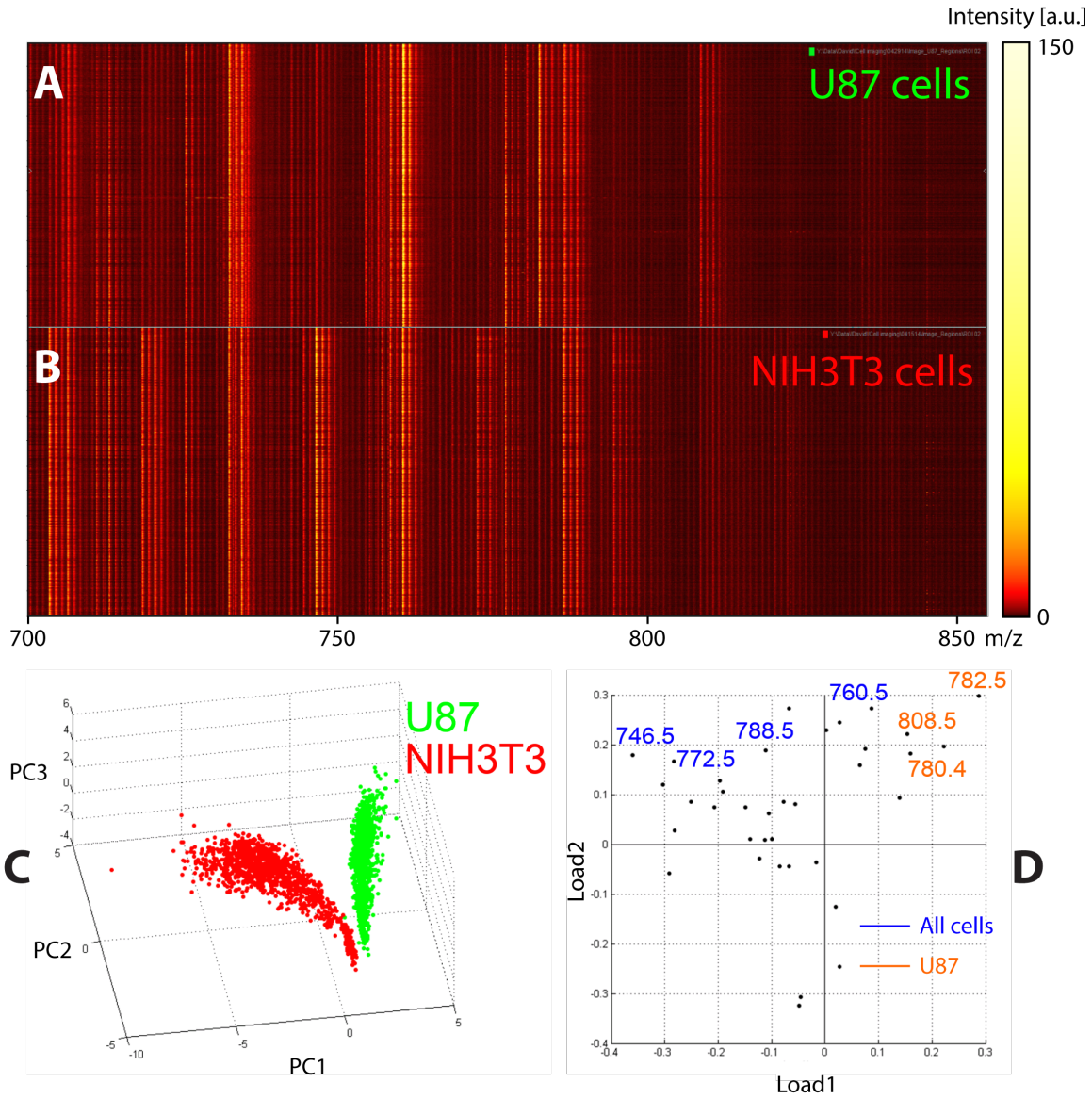

Figure 15. Phospholipid profiling in MALDI. Visualization of matrices of the phospholipid signal (700–860 Da, horizontally) across 1152 spectra (vertically) for each of U87 cells **(A)** and NIH3T3 cells **(B).** Each cell line was processed independently on a separate chip. **(C)** PCA score plot delineating the two populations. **(D)** PCA loading plot for certain mass peaks. The peaks in blue could be identified as phospholipid markers of cellularity, while the peaks in orange could be associated with U87 cells. Figure courtesy of Dr. David Calligaris, BWH

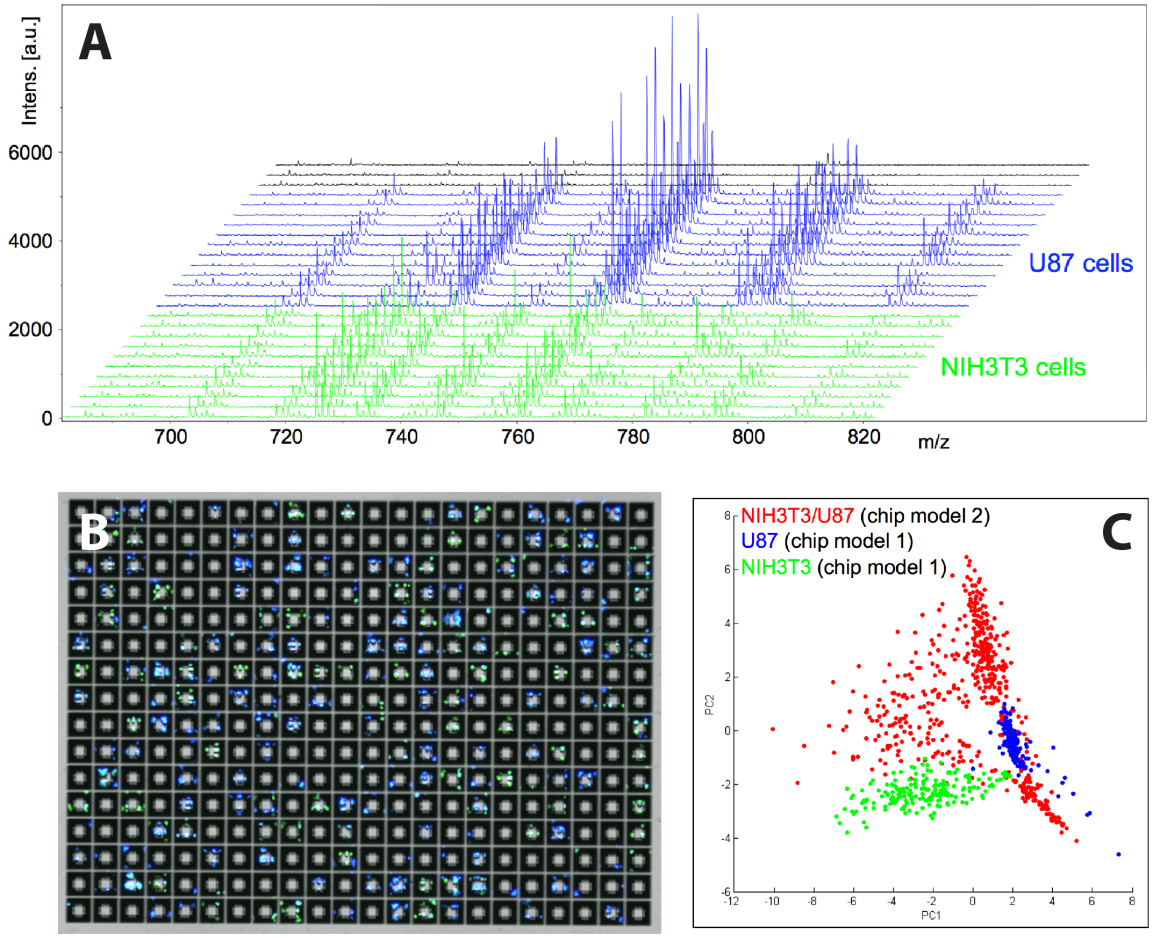

Figure 16. (A) MALDI spectra for two lines of cells processed on a single chip. **(B)** The same cells as seen in the fluorescence microscope: U87 stained with DAPI (blue), NIH3T3 expressing eGFP (green). **(C)** PCA score plot of the two populations processed separately (blue and green) or on a single chip (red). U87-specific signal (m/z 760.4, 782.4 & 808.4) can still be detected from the mixture. Figure courtesy of Dr. David Calligaris, BWH

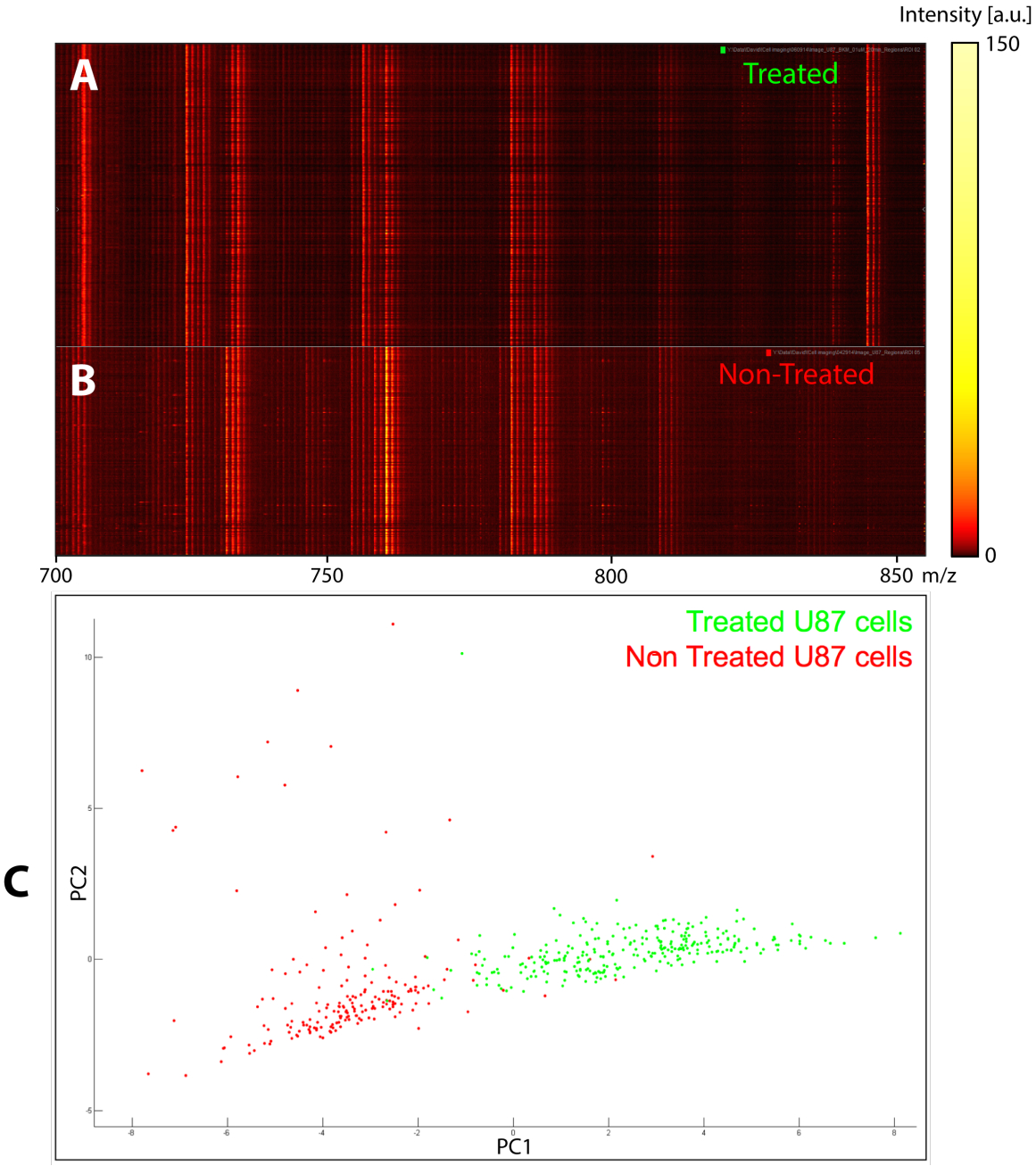

Figure 17. Comparison between 280 mass spectra of drug-treated U87 cells **(A)** and 192 spectra of non-treated cells **(B)**. PCA score plot illustrates two distinct populations **(C)**. Figure courtesy of Dr. David Calligaris, BWH

To demonstrate the ability of the assay to identify unique primary cell populations, we analyzed human primary glioblastoma cell line (U87-MG) pre- and post-treatment with lipid kinase inhibitor BKM120 (processed on separate chips). This potent drug penetrates the blood-brain barrier and acts on class I phosphatidylinositol-3-kinase (PI3K) intracellular pathway implicated in many cancers, including glioblastoma; along with its metabolites, this small molecule drug can be imaged directly (i.e. without further labeling) with MALDI MSI [57]. Although the drug has a particular molecular signature as described in [57], we have not attempted to replicate the results of that study; instead, we imaged the cells in the same m/z window as the two lines from above. Using this technique, we were able to segregate treated and untreated cells, demonstrating our ability to estimate the effect of defined perturbation (drug treatment) on the phospholipid profile of a given population of cells (**Figure 17**).

2.3 Discussion

Here we demonstrated a platform that couples fluorescence microscopy to MALDI mass spectrometry at the single-cell level. To the best of our knowledge, this is the first systematic solution to the problem of imaging large numbers of cells in a high-throughput manner using both of these imaging modalities. A unique aspect of our approach is the use of a regular array of microwells that help compartmentalize cells and image them in an organized manner. While the individual aspects of this platform have been proposed or implemented in the past, here we combined them in a single pipeline that allows for routine imaging for clinically relevant applications.

Although the mass spectrometric techniques relying on soft ionization have enabled a whole suite of “omics” studies in the last two decades, analysis at the single-cell level has remained mostly unexplored. While this disparity could be attributed to an overall lack of interest in single-cell measurements (fueled by simplifying assumptions) that until recent times permeated

the research community, we argue that technical difficulties played an equally important role. The main problems included overall low sensitivity and resolution of the instruments for such types of analyses, as well as a lack of automated pipelines that are necessary for high-throughput processing of single cells. Capitalizing on advances in instrumentation, we have developed such a pipeline and demonstrated the ability to routinely profile tens of thousands of cells at the small-molecule level. This approach complements traditional techniques that rely on labeling reagents and mainly target proteins and nucleic acids, while specific probes for small molecules may largely be inaccessible. This new imaging modality enables a more comprehensive analysis of cellular biochemistry that is necessary for understanding such complex diseases as cancer, which are accompanied by considerable changes in metabolic states of cells and cannot be resolved in enough detail at the population level. We have showcased two examples of such analyses: a study of heterogeneity of mixed samples of cells that is particularly relevant for aggressive tumors (e.g. glioblastoma) and could be resolved by lipid profiling of single cells, and characterization of drug susceptibility of a model cell line, where the single cell analysis could resolve metabolic responses to a particular stimulus.

While single-cell profiling could potentially be performed in plating experiments where the cells are simply attached to a flat surface in a chaotic manner, the use of microwells is beneficial in several aspects. First, it allows us to compartmentalize the cells, forming individual "chambers" that isolate cells from each other, reduce paracrine signaling and decrease the lateral spread of molecules that may occur during the sample preparation for MALDI (thus effectively up-concentrating these molecules to meet the sensitivity requirements of the instrument). These chambers could also enable microengraving, whereby each microwell would be sealed against an elastomeric surface that captures the secretome of each cell. Finally, the spatial arrangement of the wells in a rectangular grid streamlines image processing and registration of the locations of individual cells, which is critical for subsequent acquisition of the molecular signal in a MALDI instrument in a confident and timely manner.

Compared to other recent single-cell mass-spectrometric tools (e.g. CyTOF or microfluidic chip-based), the microwell approach tracks the history of analysis of individual cells throughout the experiment, enabling multiple modalities (microengraving, cytometry/phenotyping, metabolic profiling) to be integrated in a "passport" for each cell. It also enables analysis of limited samples, where a tissue biopsy can only have tens of thousands or fewer cells, far less than the minimum amount required for flow-based analyses with a considerable cell loss. Although CyTOF is aimed at immunophenotyping and not small-molecule analysis, it heavily relies on the use of expensive isotope-antibody conjugates as labeling reagents, which limits the applicability of this technique to the list of known targets and adds to the overall complexity of this approach. No such restriction exists for our MALDI-based pipeline; targeting various molecules can be as simple as changing the matrix.

One limitation of our approach lies in the optical imaging of the chips. The current generation of devices is not transparent, which does not allow us to easily observe and control the process of loading of cells into the wells, as compared to the case of PDMS or transparent plastics. This limitation also prevents imaging of the chips in an inverted microscope with cells resting in the wells located at the top of the chip; we have to fix cells to the chip and image it with wells facing down. Although we could use an upright microscope, it was not readily available in the MALDI imaging laboratory at the time of this writing; but more importantly, there is another problem when the objective faces the wells. Namely, the metallic surface of the chip is highly reflective, creating "ghost" images on the walls of the well around each cell (**Figure 12**). To address these issues, we propose the next version of the chip, whereby the wells would still be fabricated in silicon (preserving their shape), but their bottom would be formed by a transparent glass substrate (e.g. Pyrex), anodically bonded to the silicon wafer, while the conductive layer could be formed by thin film deposition of ITO. A sample fabrication process for such devices is described in [58]. Although more involved, it could solve the problems described above.

In all instances, the microfabrication process requires the use of cleanroom facilities,

which increases the cost and complexity of our pipeline. Although microfabrication could be made economic for batches of large wafers with many devices per substrate (and our processing steps are certainly bulk-compatible), ideally the chips produced in this way should be reused. To this end, we have evaluated a protocol regularly employed in the MALDI imaging laboratory for cleaning of ITO slides from organic residues of tissues and spotted samples (see Methods); it involves repeated sonication with a detergent and multiple solvents (we have also tried stronger detergents). Unfortunately, the prior fixation of cells to the chips leaves many partial cells attached to the chips even after this rigorous procedure; we also cannot scrub the bottoms of the wells (unlike a flat slide), and abrasion could lead to the damage to the conductive film. A more rigorous process used to remove organic residues in the microelectronic industry involves the use of piranha solution. Unfortunately, in our tests it proved to be highly corrosive to the gold film; it is also a hazardous substance, requiring careful use in minute quantities if done in a general-purpose biomedical laboratory. Our chips could function without the gold film if their surface was driven sufficiently conductive to form Ohmic contacts in the presence of native oxide. This would be possible if silicon was so heavily doped that electrons could freely tunnel through the depletion region in silicon and ~1–2 nm of oxide; the carrier concentrations required for this effect are typically on the order of 10^{19}–10^{20} cm^{-3} [59], corresponding to resistivities of 10^{-2}–10^{-3} Ohm•cm [60]. The wafers with such low resistivities are not readily available (an alternative would be to use ion implantation or diffusion to dope a surface layer). Additionally, at such high concentrations anisotropic etching rates start to decline, although they could still be practical in case of n-type doping [61].

Moreover, the MALDI process is destructive to cells. This may be disadvantageous if we want to relate phenotypes or metabolism to the genomic or transcriptomic levels, which would require recovering cells or their lysates from the microwells for sequencing. While microengraving with PDMS stamps is compatible with these downstream analyses, the MALDI analysis of cells composition has to be an endpoint. One could also develop MSI of secreted

products captured by microengraving (such as exosomes), which would not interfere with cell viability.

Although our method has been demonstrated for the analysis of phospholipid composition of cells, we believe that it could be translated to other types of molecules [35]: other lipids, cell cycle and drug metabolites, peptides and potentially even mRNA, polysaccharides, and proteins. Our approach is equally applicable to all of them, as MALDI doesn't have inherent limitations on the m/z ratio. The only substantial requirements are the abundance of the molecules and the sensitivity of the instruments to detect them. While each class of molecules requires optimization of the protocols and reagents, there is reasonable hope that with the improvement of the sensitivity of the instruments we will gain additional insight into these classes of analytes.

Finally, while we have mainly been interested in profiling of brain tumors (and the information about specific lipid profiles might have been already available for them), our approach can be broadened to other classes of cells and diseases. Information about cellular heterogeneity is equally important for other types of cancer, immune profiling, studies of the gut microbiome and bacterial infections. Systematic, comprehensive and rapid methods for obtaining this information can greatly benefit not only our understanding of the progression of cell populations and associated diseases, but can provide clinicians with valuable input affecting their decisions at the bench side.

2.4 Methods

Mask design was performed using an in-house Perl script and an official DXF Reference specification [62] for the open file format used by Autodesk AutoCAD. The files could be generated by the script in 10–20 sec and checked for consistency in AutoCAD. All features were "drawn" as non-intersecting closed polylines to meet the requirements for plotting set by the masking companies. The final file was converted from DXF to GDSII format and checked in Bay

Technology LinkCAD. The file was then sent for production to Photo Sciences Inc.; the mask was made on a 7" soda-lime glass at CD 3um, with clear features, chrome side down.

Fabrication of the Si chip was carried out in class 10 (the Integrated Circuits Laboratory, ICL) and 100 (the Technology Research Laboratory, TRL) cleanroom facilities of the Microsystems Technology Laboratories (MTL) at MIT. 6" <100> Si wafers (prime grade, CZ, N-type Phos., resistivity 4–7 Ohm-cm, thickness 600–650 um) were supplied by MTL from MEMC Electronic Materials. LPCVD silicon nitride was deposited by MTL staff in SVG/Thermco 7000 Series vertical thermal reactor (VTR). Photoresist processing was performed on automated SSI 150 coater/developer track ("coater6") using a standard recipe; briefly, wafers were treated with hexamethyldisilazane (HMDS), and SPR700 v1.2 positive photoresist was spun-on for ~1 um thickness and pre-baked at 95C. The photoresist was exposed for 5 sec in Electronic Visions 620 mask aligner; no precision alignment was necessary, but the mask and the wafer flat were assured to not be askew relative to each other. The photoresist was then developed with in-line developer on coater6. The silicon nitride was dry-etched for a total of 120 sec with SF_6 plasma in Lam Research Model 490B. The photoresist was stripped with piranha solution, a 1:3 mixture of 30% hydrogen peroxide (H_2O_2) to concentrated sulfuric acid (H_2SO_4) (acid first), for 10 min. Anisotropic wet etching of Si was performed with 20% wt. solution of potassium hydroxide (KOH) in water at 80C for ~50 min to achieve ~50 um deep wells. The quality of etching was inspected in a reflected light microscope. Wafers were cleaned from KOH with a double-piranha protocol (10 min piranha, rinse in DI water, 10 min piranha, dump-rinse) as a requirement to use the next (CMOS-compatible) acid hood. The remaining silicon nitride was stripped with 85% wt. phosphoric acid at 165C for 20 min. Finally, Sloan 8KV electron-beam evaporator was used to deposit 10nm of Ti and 100nm of Au. The wafers were then cut to individual chips using Disco Abrasive System Model DAD-2H/6T die saw.

The plastic chips were made by Edge Embossing LLC from a master with the use of two intermediate elastomeric molds. The master consists of SU-8 posts patterned on a 4" Si wafer

using standard photolithography performed at the Institute of Electronics and Nanotechnology of Georgia Institute of Technology; the masks were ordered from Photo Sciences Inc. with dark features, chrome side down. ITO and Au were deposited on plastic chips in AJA Orion 5 sputtering system at class 10,000 (the Exploratory Materials Laboratory, EML) facility at MTL.

Characterization of the chips with scanning electron microscopy was performed in secondary electron mode at low kilo-voltage on general-purpose microscopes, either JEOL 5910 at the MIT Center for Materials Science and Engineering (CMSE) or JEOL 6010LA at the MIT Institute for Soldier Nanotechnologies (ISN).

Cell preparation. NIH3T3 (mouse fibroblast) cell line was engineered to express enhanced green fluorescent protein (eGFP) reporter gene by Dr. Salil Desai at MIT. U87-MG (human primary glioblastoma) cells (ATCC) were stained with 50 ug/mL 4',6-diamidino-2-phenylindole (DAPI, Invitrogen D21490) nuclear stain for 1 min and washed 3 times in 1x PBS to remove excess dye. NIH3T3 and U87-MG were cultured in Dulbecco's Modified Eagle's Medium (DMEM) (Fisher Scientific) with 10% fetal bovine serum (FBS), 1% Penicillin-Streptomycin and 1% L-glutamine (Life Technologies). The cells were counted on a hemocytometer and re-suspended in 1x PBS to the final concentration of ~50,000 cells/mL. The chip was treated for 5 min in Harrick PDC-001 plasma cleaner, and 1 mL of cell suspension was spread across the useful area of the chip. The cells were allowed to settle for 3 min, after which the chip was rotated 180° to even out a possible tilt, and was allowed to stay for 3 more min. For the drug response experiments, U87-MG cells were incubated on the chip with 5 uL of 100 uM BKM120 in DMSO for 20 min at 37C. The chip was then slanted on a dish, and 500 uL of 1x PBS was gently run from the upper short edge to wash out excess cells; this washing was repeated for alternating sides 5–10 times. The remaining cells were fixed for 15 min with 0.25% glutaraldehyde in 1x PBS at 37C. Finally, the chip was washed 5 times for 2 min in DI water to remove salts and dried in a MiniArray Microcentrifuge (VWR) for 5 min.

Imaging cytometry was performed on AxioObserver Z1 with AxioCam MRm Rev.3 and

a 5x, 0.16 NA objective from Zeiss. The camera sensor has 1388 x 1040 pixels, each 6.45 um in size. A 0.63x de-magnifying lens installed before the camera enabled the total magnification of 3.15x. The total field of view was then (1388 x 1040) * 6.45 um / 3.15 ~ (2842 x 2130) um, imaged at 6.45 um / 3.15 ~ 2.05 um/pixel; the Abbe diffraction limit at 500 nm is 0.61 * 0.5 um / 0.16 ~ 1.9 um, optimally close to this theoretical resolution. Each block of wells was designed as (2700 x 2000) um rectangle to provide an overlap for subsequent stitching; a typical geometry of the chip had 21 * 9 = 189 blocks. The block-by-block acquisition was set up in ZEN software environment, with spline interpolated focus based on a 5 x 3 grid of focal support points. The microscope had been equipped with a rotating turret of fluorescence filters mounted in cubes; a bright-field reflected light cube was set up with 10:90 UVFS plate beamsplitter (Thorlabs, BSN10R) and an OD 4.0 AR-coated neutral density filter (Thorlabs, NE40B-A). Imaging of all blocks with 3 channels (bright-field, DAPI, eGFP) took less than 10 min.

Image processing was carried out in MATLAB-based Enumerator software written by Dr. David Biggs, taking ~15 min on an 8-core Xeon CPU with 64GB RAM. The software outputs a '.cells.txt' file containing a tabulated list of positions of detected cells.

Matrix deposition. An in-house sublimation apparatus was engineered by Dr. David Calligaris at BWH (**Figure 18**). 300 mg of α-cyano-4-hydroxycinnamic acid was dispensed at the bottom of the glass jar. The chip was tape-mounted to the glass insert and placed ~ 2 cm above the matrix crystals. The jar and the insert were sealed with an o-ring, and the resulting chamber was evacuated to 20 mTorr (a cold trap before the pump was used to condense any dangerous vapors from sublimation). The assembly was placed on a heated sand bath at 140 C, and the insert was filled with ice at 4 C. The sublimation was allowed to proceed for 20 min. After the sublimation, the chip was placed face down on a metal holder installed in a glass chamber that was filled with 50% methanol and 5% acetic acid in water, and left at 85C for 10–20 min to co-crystallize the matrix with the lipid molecules.

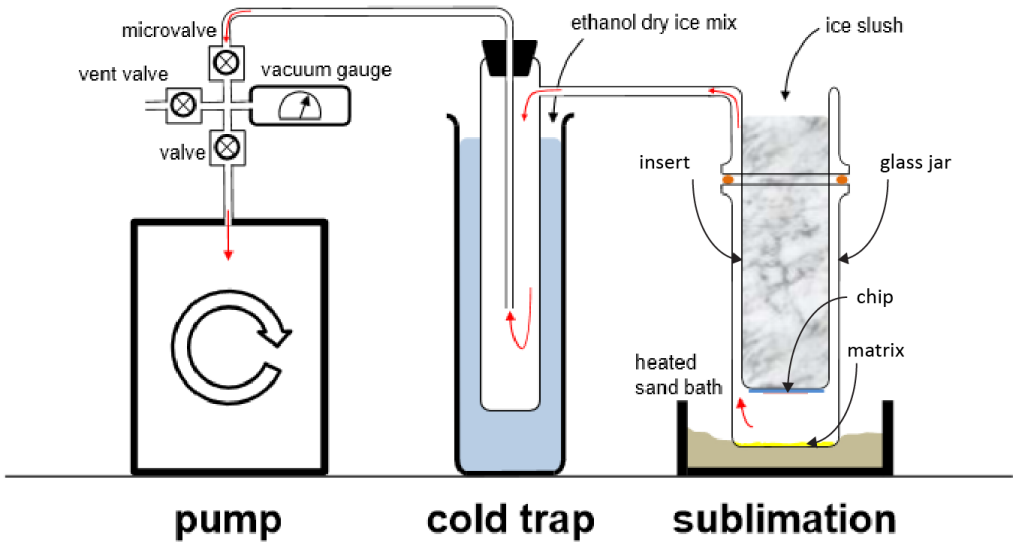

Figure 18. Schematics of the sublimation apparatus used for deposition of the matrix. Figure courtesy of Dr. David Calligaris, BWH

Registration. The chip was mounted in a specimen holder (designed to accommodate microscope slides) and was placed in the MALDI instrument. With the help of an in-house MATLAB script, the individual images of the blocks were extracted and downscaled from ZEN file, the fluorescent and bright-field channels were artificially colored and were overlapped, and the final images were stitched and fused together using the Grid/Collection Stitching plug-in from Fiji/ImageJ on the image processing workstation. The final uncompressed size of the image was set to no more than 200 MB to be compatible with MALDI imaging software flexImaging 4.0 (Bruker Daltonics). The image was also flipped in ImageJ to show the actual (not mirrored as imaged) surface of the chip, where the labeling numbers looked right. In several instances of the experiment, stitching missed a corner block, in which case we used ImageJ to draw the position of the corner well of that block. We began a "Tissue Profiling" experiment in flexImaging and, using the live window, navigated to the corner wells of 3 corner blocks on the chip, and matched them to those in the image. The dummy experimental XML file containing this calibration information, along with the '.cells' file from Enumerator and the stitched image file, were then

imported into a custom Python script that calculated the absolute positions of all the wells with the cells, along with a fraction of empty wells, and added them to the XML file, displaying the results as dots on the image for visual inspection (**Figure 13**). The updated XML file was then imported back to flexImaging.

MALDI imaging was performed on Bruker ultrafleXtreme in reflectron positive ion mode. The spectra were calibrated using a standard solution pre-spotted at the edge of the chip. The laser probe spot diameter was normally set to 50 um to match the size of the bottom of the wells. The beam was manually offset to compensate for the variation in height between the bottom and top surfaces of the wells. For each position, 1000 laser shots were fired with a small "random walk" and accumulated into one spectrum. Acquisition took ~3–4 h for a typical chip with ~18,000 wells.

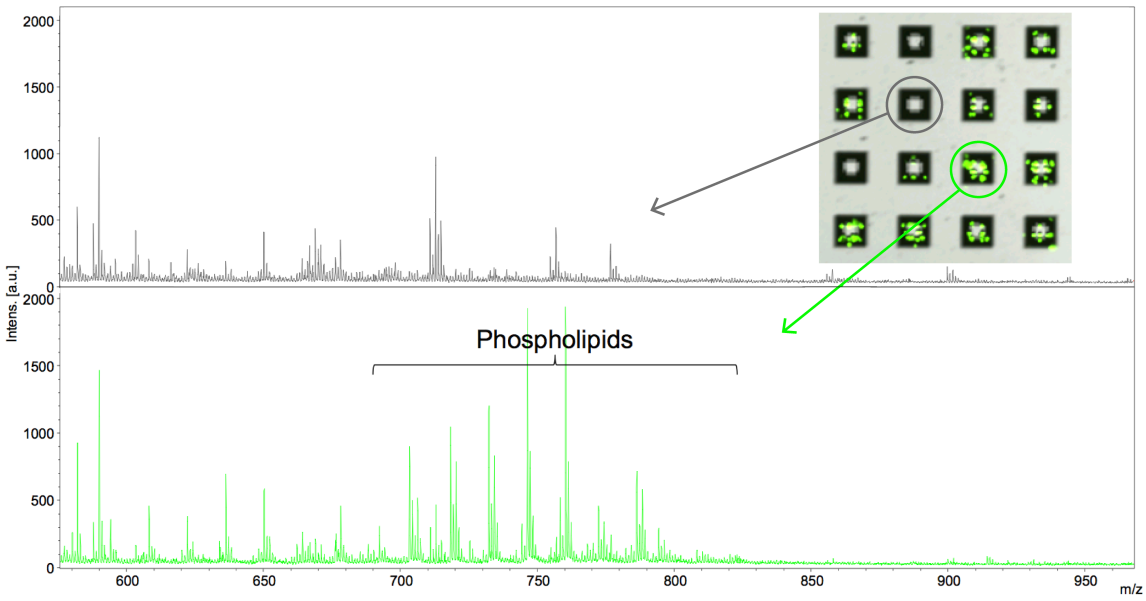

Figure 19. Detection of phospholipids from NIH3T3 cells. Green spectrum corresponds to wells with cells, gray – empty wells (as detected by fluorescence). Figure courtesy of Dr. David Calligaris, BWH

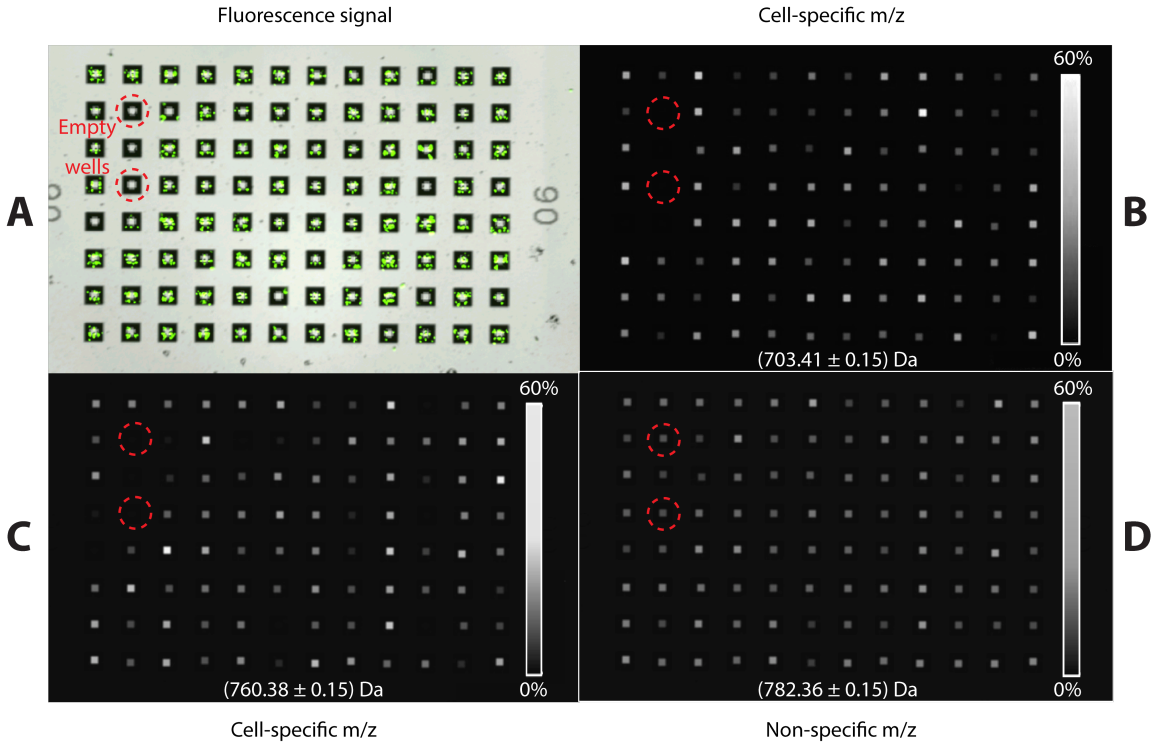

Figure 20. Cell-specific **(B, C)** and non-specific **(D)** MALDI signal, as compared to fluorescence **(A)**. Red circles indicate locations of empty wells. Courtesy of Dr. David Calligaris, BWH

MS analysis started with a manual observation of characteristic peaks in the region of interest (e.g. 700 – 800 Da for phospholipids) for the spectra located on wells with the cells as compared to empty wells. The peaks present in the former but absent in the latter (**Figure 19**) were then visualized on the image of the chip, with mass filters set to +/- 0.1 Da (**Figure 20**), to confirm correlation with the presence of cells. Alternatively, the peaks of interest could have been identified from the previous experiments and/or the literature. For each peak, its intensity across all the wells could be exported as a list.

To plot a ROC curve for MALDI signal with fluorescence as the gold standard (**Figure 14**), we calculated the true positive rate TPR = TP / (TP + FN), where TP were true positives (number of wells with both fluorescence and MALDI signal above a threshold), FN were false negatives (wells with fluorescence but no mass signal), versus false positive rate FPR = FP / (FP + TN), where FP were false positives (no fluorescence but mass signal above a threshold) and TN

were true negatives (no fluorescence, no mass signal), for varying thresholds.

Principal component analysis (PCA) to identify subpopulations of cells based on the MALDI signal was performed in ClinProTools 3.0 (Bruker Daltonics). The software automatically performed normalization, baseline subtraction, peak picking and recalibration of the spectra based on the default method. The mass range for PCA was set to m/z 700–1400.

Cleaning of chips from matrix and cells or their residues was attempted using an in-house protocol previously used for tissue samples fixed to ITO-coated slides. Briefly, the chips were loaded in a metallic holder for glass slides and sonicated in acetone for 15 min. After rinsing 2 times with water, we sonicated the chips further in 5% Micro-90 cleaning solution (Cole-Parmer) for 15 min. After rinsing in water again until no bubbles from Micro-90 remained, we sonicated the chips in water for 5 more min, then in methanol for 15 min, and finally in water again for 15 min.

3. Nanowell plates for cytometry and recovery of single cells

3.1 Introduction

Single-cell analysis has transformed our understanding of biology at the functional and genomic levels. Important recent applications of single-cell technologies include profiling of human immune responses [63], screening highly-secreting cells for the production of monoclonal antibodies and other biologics [43] [64], detection of circulating tumor cells (CTCs) responsible for metastatic cancers [65], and many others.

Existing platforms for single-cell analysis such as flow cytometry [66] and Fluidigm C1 [67] have been enormously useful for characterizing populations of single cells. Flow cytometry is suited to rapid acquisition of measurements of cell lineage, protein secretion, proliferation or cytolytic activity in large populations (10^6 – 10^7 at up to 10^4 cells/s) [2], while Fluidigm C1 is used for highly reliable genetic analyses on a small number of cells (96). Unfortunately, these tools still have limited potential for characterization and recovery of *rare* cells. Flow cytometry allows for routine detection of cells down to 1:1,000 [2], while Fluidigm C1 provides no mechanism for cell selection. Many important applications cited above require routine identification and interrogation of 1 in a few 10,000s of cells.

In addition, human clinical research often involves limited specimens or material for analysis; important examples include stem cells, tumor biopsies, mucosal brushes and other samples where, unlike in blood draws, only a limited number of cells of interest (10^4 – 10^5) may be available [2]. These specimens may not be amenable to the more traditional tools such as flow cytometry (which requires higher numbers of cells), and often allow only one run of analysis per sample.

Arrays of microwells have offered an alternative solution to compartmentalize single cells for high-content multi-dimensional analysis of such samples [68]. This technology enables correlation of multiple measurements involving both phenotype and genotype that can be

performed either on-chip or off-chip in a single pipeline, establishing a platform for integrative single-cell analysis [2].

Yet, the throughput of such assays remains a major limitation. While techniques such as microengraving involve up to ~10^5 cells per one array [13], the times spent on imaging, the cell loading efficiency and the number of samples that can be processed simultaneously or within a single modular operation, can certainly be improved. In addition, interfacing these custom tools with existing equipment is problematic. Finally, the mass production of such devices would greatly empower single-cell research, but is not easily achieved with the current choice of materials, such as PDMS.

Here we built a microwell platform for high-throughput cytometry and recovery of rare single cells that offers significant improvements in all these directions and has direct implications for human clinical research.

3.2 Results

Existing arrays, such as those used in microengraving [13], have relied on formats designed to interface with tools for standard microarray slides (25 mm x 75 mm), or custom formats (e.g. slabs cut out of PDMS). To accommodate increased numbers of samples processed in each modular operation, and expand compatibility with automated equipment used for these operations (liquid handlers, robotic macro- and micromanipulators, optical equipment etc.), we designed a new array that relies on the form factor of the microtiter plates. This standard – SBS format (named after the Society for Biomolecular Screening [69]) – provides compartmentalization of multiple samples on a single plastic device using an array of macroscopic wells ("macrowells") (**Figure 21**A) .

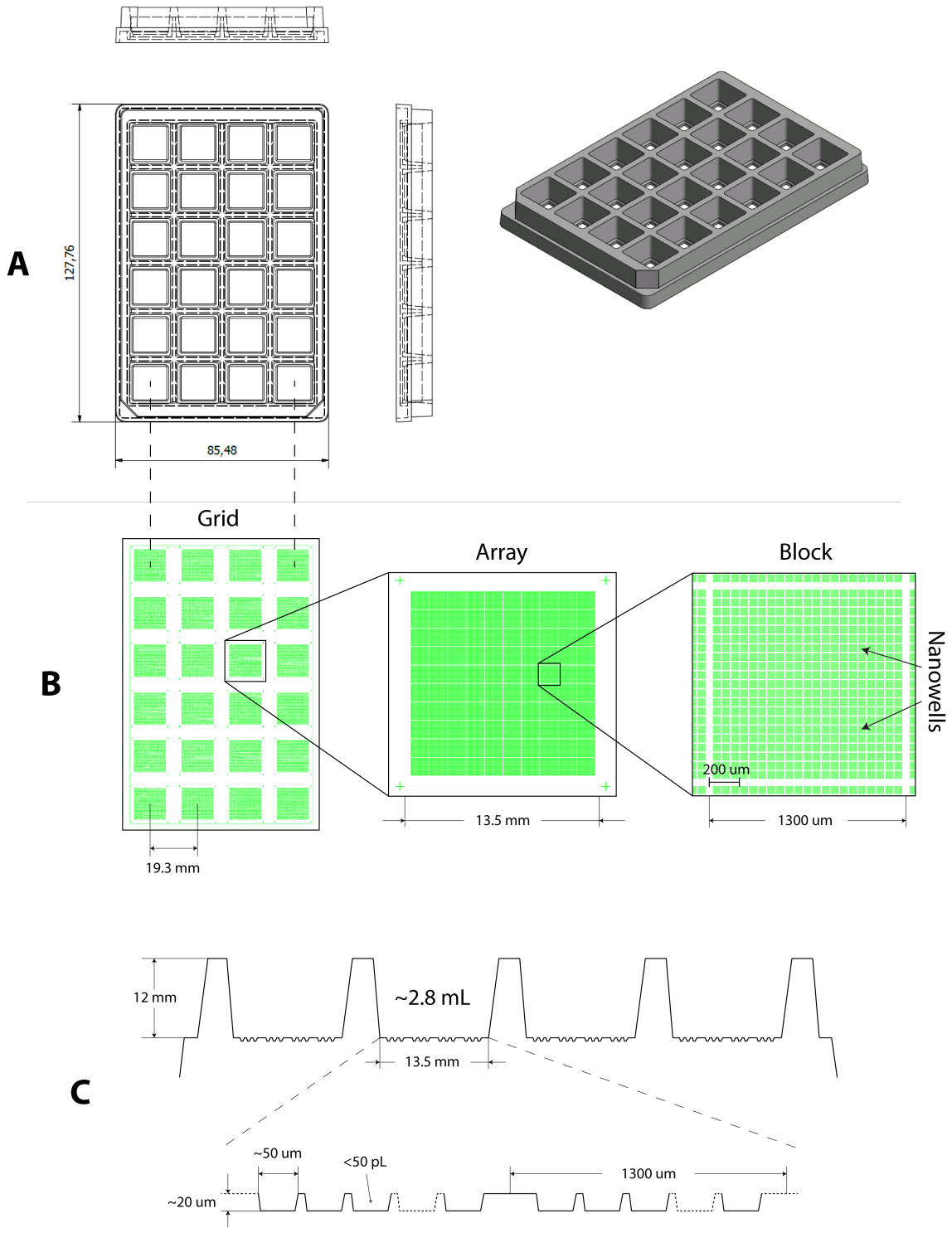

Figure 21. Design of the nanowell plate. **(A)** Schematics and dimensions of the macrowell piece (upper part). **(B)** Design of the grid of nanowells (bottom part). **(C)** Relative dimensions of the macro- and nanowells.

The second part of the device comprises arrays of microscopic wells (henceforth referred to as "nanowells" because of their sub-nanoliter volume) arranged in a grid matched to the arrangement of the macroscopic wells (**Figure 21**B). Each array of nanowells resides at the bottom of a macrowell and allows for microscopic compartmentalization of cells from the corresponding sample (**Figure 21**C).

Both parts of the device can be manufactured independently of each other, allowing additional flexibility not readily achieved with a single-piece geometry. Since we intend to ultimately mass-produce such devices for the benefit of our laboratory and a broader impact in the research community, we need to ensure that each part can be reliably manufactured according to its specific set of dimensions and tolerances, which are vastly different for the macro- and the microscale. To demonstrate the utility of these devices prior to mass manufacturing, we have chosen a number of rapid prototyping tools suitable for the production of each part. These tools allowed us to produce dozens of devices in rapid iterations to evaluate and achieve an optimal set of geometries. 3D printing and stereolithography (SLA) are fast, accessible and relatively inexpensive additive technologies for building macroscopic pieces where high resolution is not required [70]. The microscopic part can be replicated with soft embossing [52] from a rigid master that is fabricated once in a standard cleanroom facility.

We evaluated two processes for the production of the masters. In one instance, we used anisotropic etching of Si for the microfabrication of nanowells with tapered walls [56] (see Chapter 2). This geometry facilitates replication of the rigid master in a subsequent molding step, as the draft angle of ~35^0 (defined by crystalline planes in Si [56]), along with an extremely low surface roughness produced by the process, aid separation of the molded piece from the master (**Figure 23**A, left). Additionally, such wells could be moved closer to each other, while maintaining the overall thickness and rigidity of the walls in between, which could otherwise deform or collapse upon replication in plastic had the walls been vertical (e.g. for 10 um nominal width and 20–35 um depth of the walls); see **Figure 23**A, right for comparison. Close separation

between the wells maximizes the useful area of the device (allowing us to fit more wells in a smaller area), increasing the number of samples that could be processed on each device, decreasing imaging times per sample and minimizing cell loss due to the "dead" area (so that a larger proportion of cells could settle into the wells from suspension). Additionally, such close separation could not have been achieved with the older method of production of the masters, namely with SU-8 posts photolithographically patterned on a Si wafer, as close spaces between the posts necessitated longer development times to remove residual photoresist, which could result in distortion of the features.

Alternatively, we employed deep reactive-ion etching (DRIE) of Si to produce masters with vertical walls [71] (**Figure 22**, **Figure 23**B,C). Briefly, we defined patterns of microwells in ~10 um thick photoresist on Si wafers. We then employed the Bosch process, which applies alternating cycles of chemically reactive plasma and sidewall passivation gas to produce deep structures with almost perfectly vertical profile of the walls [71]. However, one side effect of this process is an undulating profile of the sidewalls (**Figure 23**C, bottom-right), which may complicate subsequent molding due to additional friction. To reduce the impact of this effect, as well as to prevent deformation of the features upon molding while keeping the distances between wells short, we decreased the depth of the wells relative to their width (**Figure 23**B, left). One advantage of vertical walls over the trapezoid profile described above is an increased area at the bottom of the wells (**Figure 23**B, right); it will come useful when we consider loading wells with magnetic beads that can occlude the field of view at the bottom of the wells if the area is not large enough. After the Bosch process, we stripped photoresist and could additionally passivate the sidewalls in the same instrument to aid separation of microstructures subsequently molded from the primary or secondary masters.

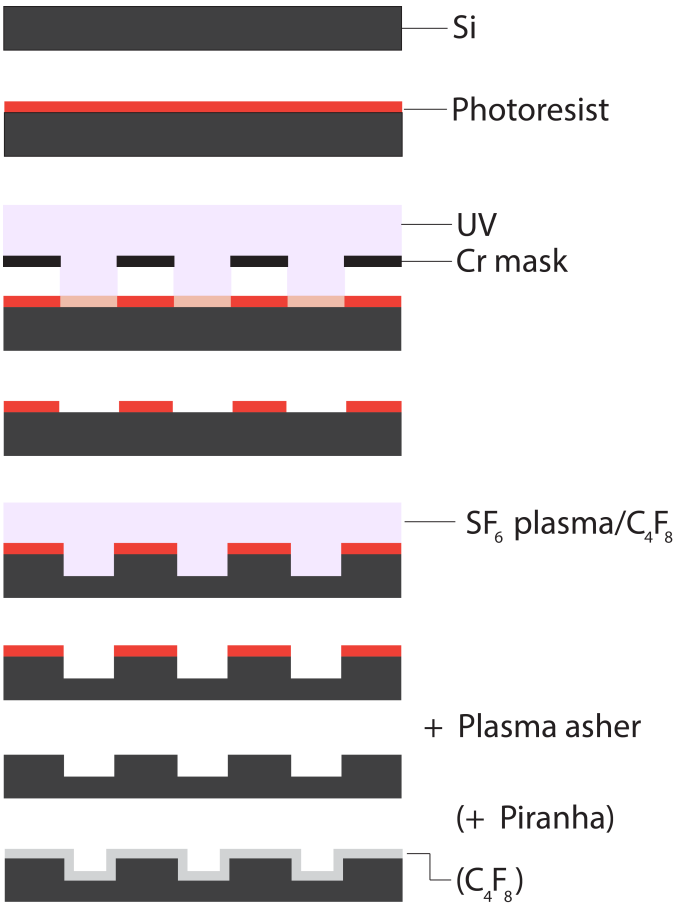

Figure 22. Steps for microfabrication of masters with DRIE.

Both of the techniques described above employ bulk micromachining of Si, ensuring that microscopic features are a single piece with the wafer, unlike in the processes where the features are attached to the wafer and may wear out with repeated moldings (an example of such process is patterning of SU-8 posts).

To facilitate image acquisition and analysis, we arranged the nanowells in blocks that fit the field of view on the microscope (see Methods); if the blocks were spaced further apart, the separation area would be unused in cell loading (potentially resulting in cell loss), while a shorter distance between the blocks would increase the number of blocks per given area, thus increasing the time spent on imaging. Within each block, we tried to fit as many wells as possible, while accounting for a possible drift of the microscope stage from one block to another (**Figure 30**), which may lead to incomplete imaging of the outermost wells.

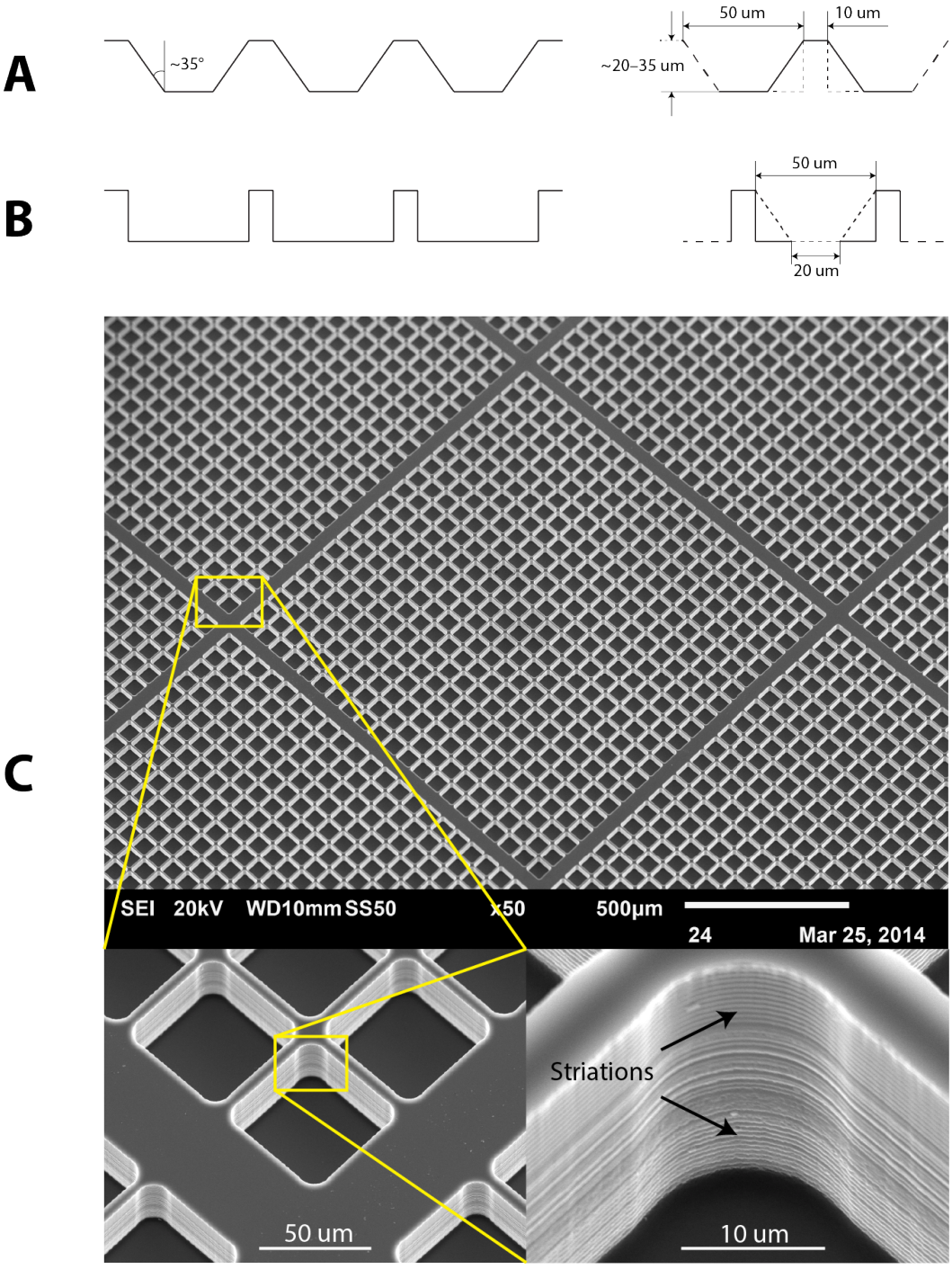

Figure 23. Alternative designs of nanowells. **(A)** Nanowells produced with anisotropic etching of Si. **(B)** DRIE of wells with vertical walls. **(C)** SEM images of nanowells produced with DRIE.

To reduce cell loss, the edges of each array of nanowells (corresponding to one macrowell) were designed to be as close as possible to the edges of the macrowell. However, since the two parts of the final device have different tolerances on the materials and processes involved in their production, and they have to be aligned and bonded, we cannot rely on a microscopically precise alignment. As such, we had to introduce a ~200 um border gap at the edges of each array. Additionally, to be able to access the outermost wells with macroscopic tools such as a liquid handling pipette or a cell picking capillary, as well as to facilitate molding of the macrowell plate in the future, we introduced a taper to the sidewalls of each macrowell.

A typical workflow for finished devices (**Figure 24**) is illustrated in **Figure 25**. It starts with a suspension of fluorescently labeled cells drawn from a clinical sample (this could be a disaggregated tumor, a tissue biopsy, whole blood etc.). We then load cells from each suspension into the nanowells of a corresponding macrowell, which could be accomplished in a number of ways (settling by gravity, centrifugation, immunomagnetic enrichment etc.). We proceed with automated imaging of each array in a block-by-block fashion, and then process the results with a semi-automated image analysis software. This analysis produces a list of candidate cells with their locations that could then be used to transfer individual cells of interest to the wells of a 96-well plate for downstream analysis (such as transcriptional profiling, whole exome sequencing, or clonal expansion).

To assess the utility of this expanded format for a variety of single-cell analyses, we designed experiments for identification and recovery of rare cells and for phenotypic analysis of small clinical samples.

Figure 24. Nanowell plate for single-cell cytometry.

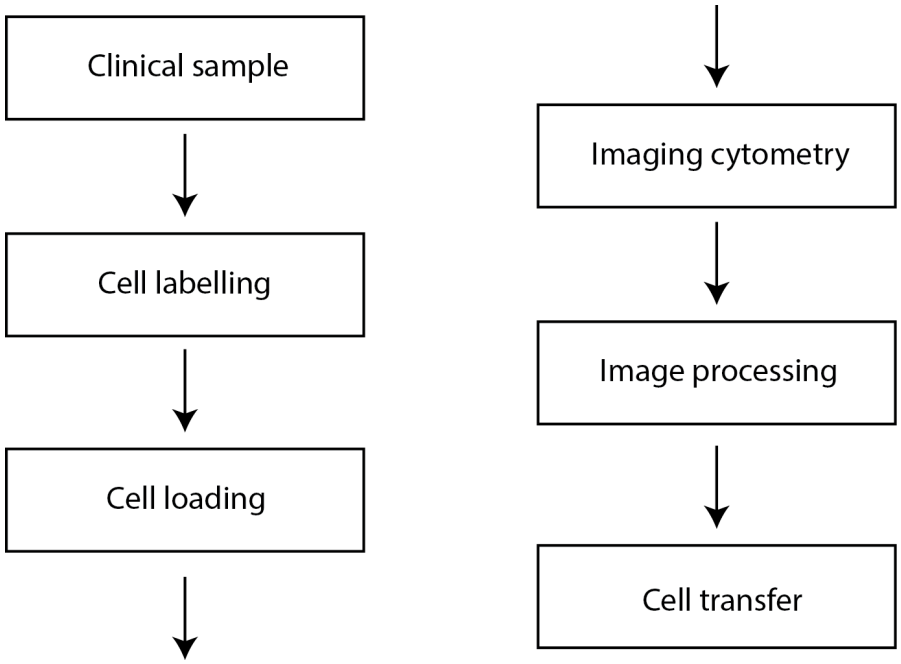

Figure 25. Workflow for single-cell analysis using the nanowell plates

3.2.1 Identification and recovery of CTCs

Circulating tumor cells (CTCs) are rare tumor cells found in the blood of cancer patients (~1 ppm mononuclear cells) and believed to be responsible for disseminating cancer (metastasis) [72]. The numbers of CTCs found in blood can serve as a prognostic indicator in certain tumor types [73]. While a variety of methods for enriching and enumerating CTCs have been developed over the past decade (most notably CellSearch, the only *FDA-approved* method for this purpose [73]), CTCs offer many opportunities beyond enumeration. Indeed, molecular analysis of CTCs may reveal information about solid tumor lesions and allow monitoring of the progression of disease from blood samples. Along with the analysis of circulating tumor DNA, such "liquid biopsies" offer a real-time, minimally-invasive window into metastasis that would not be feasible using repeated surgical biopsies [74], [75].

Sequencing-based analyses of CTCs should allow us to trace lineage-specific evolution of tumors, assess clonal heterogeneity, and reveal mechanisms of resistance to therapies [72]. However, the inherently small amount of material available from each cell (e.g. only 1 copy of each parental allele) necessitates the use of amplification methods prior to sequencing that introduce biases and errors which confound the confident calling of mutations and copy-number alterations [76]. Census-based methods enable accurate and powered calling of somatic alterations from CTCs, but require isolating, amplifying, and sequencing multiple independent CTCs, and thus are limited when an insufficient number of cells is available [76]. As such, increasing the number of single CTCs recovered from a given volume of blood (or processing larger volumes in a given time) is paramount to performing more confident and detailed analyses, along with expanding the (sometimes incompatible) types of analysis performed on each sample.

A substantial number of methods for detection, enrichment and limited characterization of CTCs have been developed over the last several years [77]. These methods can generally be divided into marker-dependent and marker-independent. The former mainly relies on specific

proteins displayed on the surfaces of CTCs and not white blood cells—or vice versa. Positive selection relies upon epithelial cell adhesion molecule (EpCAM) expression on CTCs and negative selection relies upon expression of CD45 on white blood cells. These antigens are targeted by antibodies conjugated to fluorophores or magnetic beads to selectively enrich or deplete a sample for cells expressing them. Some recently developed technologies (such as microfluidics-based CTC-iChip [78]) can operate in either mode of selection to increase total enrichment rates. When target cells do not express specific or known markers, marker-independent methods relying on physical differences between malignant and normal cells are used, such as filter-based isolation by size of epithelial tumor cells (ISET) [79] or ScreenCell [80].

After the sample is enriched and CTCs are identified, they still need to be recovered for further analysis. Recoveries are mainly performed by FACS, microfluidics, laser micro-dissection or micromanipulation [72]. Each method has its own advantages and flaws, but for image-guided recovery, micromanipulation is the most straightforward of all. However, it is still generally performed through time-consuming manual micromanipulation, or in rare cases in automated fashion when suitable equipment (such as ALS CellCelector [81]) is available.

Here we leveraged the new format of the nanowell arrays to integrate enrichment with the automated platform established for CTC identification and recovery [76]. We developed a method for on-chip enrichment that combines immunomagnetic labeling with density gradients (**Figure 26**). Lysis of red blood cells (RBCs) is performed on a vial of blood, and the resulting cell suspension is then incubated with immunomagnetic beads to selectively label EpCAM-expressing CTCs. Macrowells of our plates are filled with a biocompatible dense medium such as Percoll (colloidal suspension of silica nanoparticles coated with polyvinylpyrrolidone), and the bead-labeled cell suspension is dispensed on top of it; the two liquids remain separated according to their densities. Since the beads are much heavier than the cells or the medium (e.g. iron has 6–7 times higher density), and a few of them are conjugated to each cell, they can pull CTCs

through the dense layer by gravity. Additionally, these cells can be pulled with a magnet placed underneath the imaging surface (**Figure 26**a). As a result, CTCs sediment into nanowells at the imaging surface, but only a few contaminating WBCs ever reach the same level.

After sedimentation, we can aspirate the blood layer and the dense medium, which removes the majority of contaminating WBCs or remnants of RBCs. We then wash and stain cells on the magnet, remove the latter and image cells on the same surface (**Figure 26**a, right). CTCs selected based on positive and negative fluorescent markers and morphology can be subsequently recovered by automated micromanipulation to a PCR plate for whole-genome amplification, library preparation, and sequencing, as described elsewhere [76].

To validate CTC recovery rates for this platform, cells from a cancer cell line were fluorescently labeled and manually counted on a glass microscope slide (**Figure 26**b). We then spiked the same amount of cells (per volume) into RBC-lysed, healthy donor blood, and processed these spiked samples via the procedure described above (**Figure 26**a, b). We determined the numbers of cells recovered based on the imaging cytometry (**Figure 26**c). The chart in **Figure 26**c demonstrates the rates of recovery that decrease with volume of processed blood, but are still fairly high even for greater volumes (> 7.5 mL).

The new format allows us to directly perform enrichment on nanowell arrays using the macrowells to partition the samples, which would not be straightforward with the old design (in the format of a microscope slide). We also compared cell recovery rates between the two platforms. A schematic of this study is shown in **Figure 27**A (we didn't perform immunomagnetic enrichment for a more clear comparison, since the old design doesn't natively accommodate it). Recovery rates proved to be very similar for both platforms (**Figure 27**B). The imaging times, however, were substantially lower for the new design, suggesting an overall improved efficiency in processing rare cells such as CTCs (see Discussion and Methods).

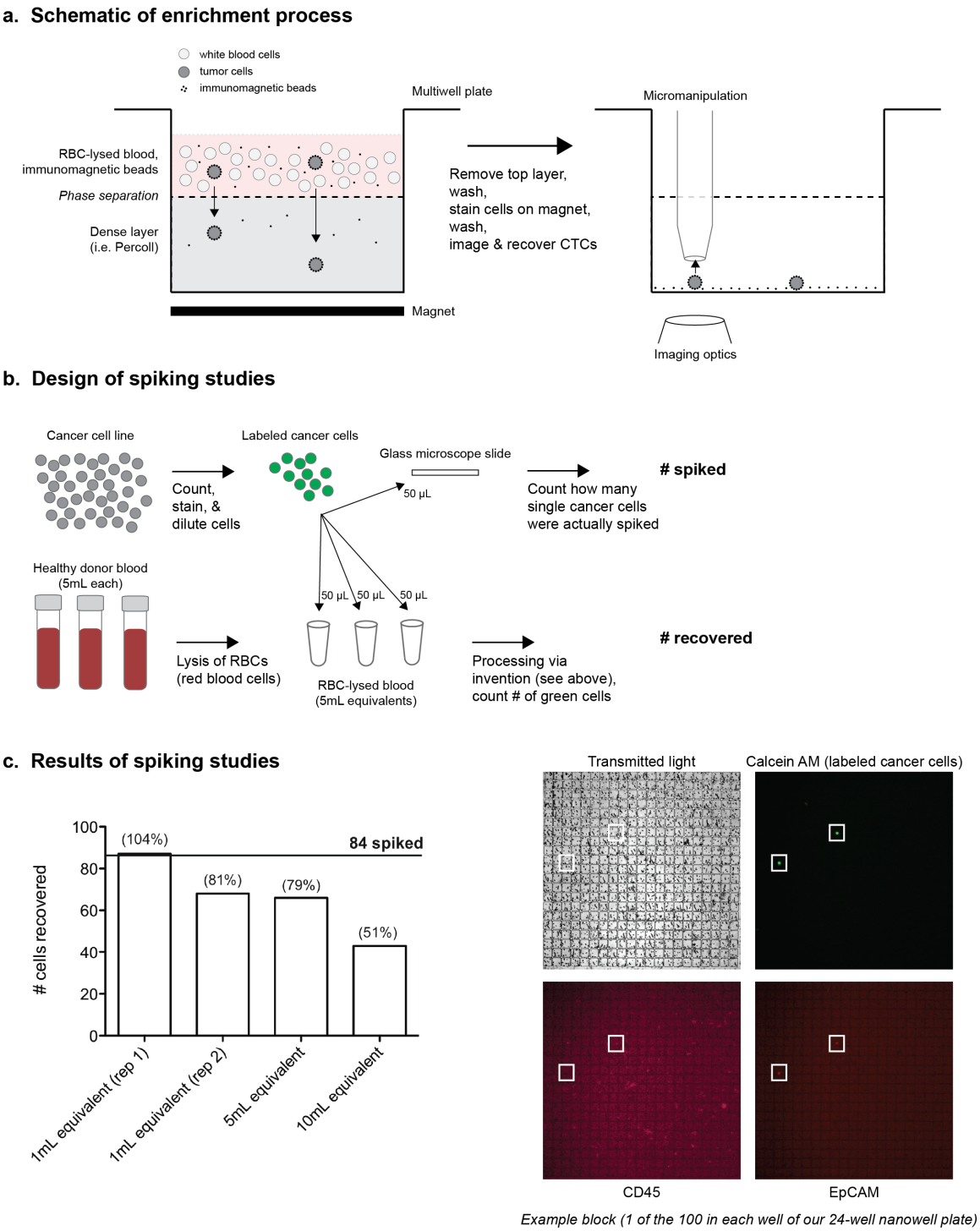

Figure 26. Direct density-based immunomagnetic enrichment and recovery of CTCs using the nanowell plates. Figure courtesy of Viktor Adalsteinsson, MIT.

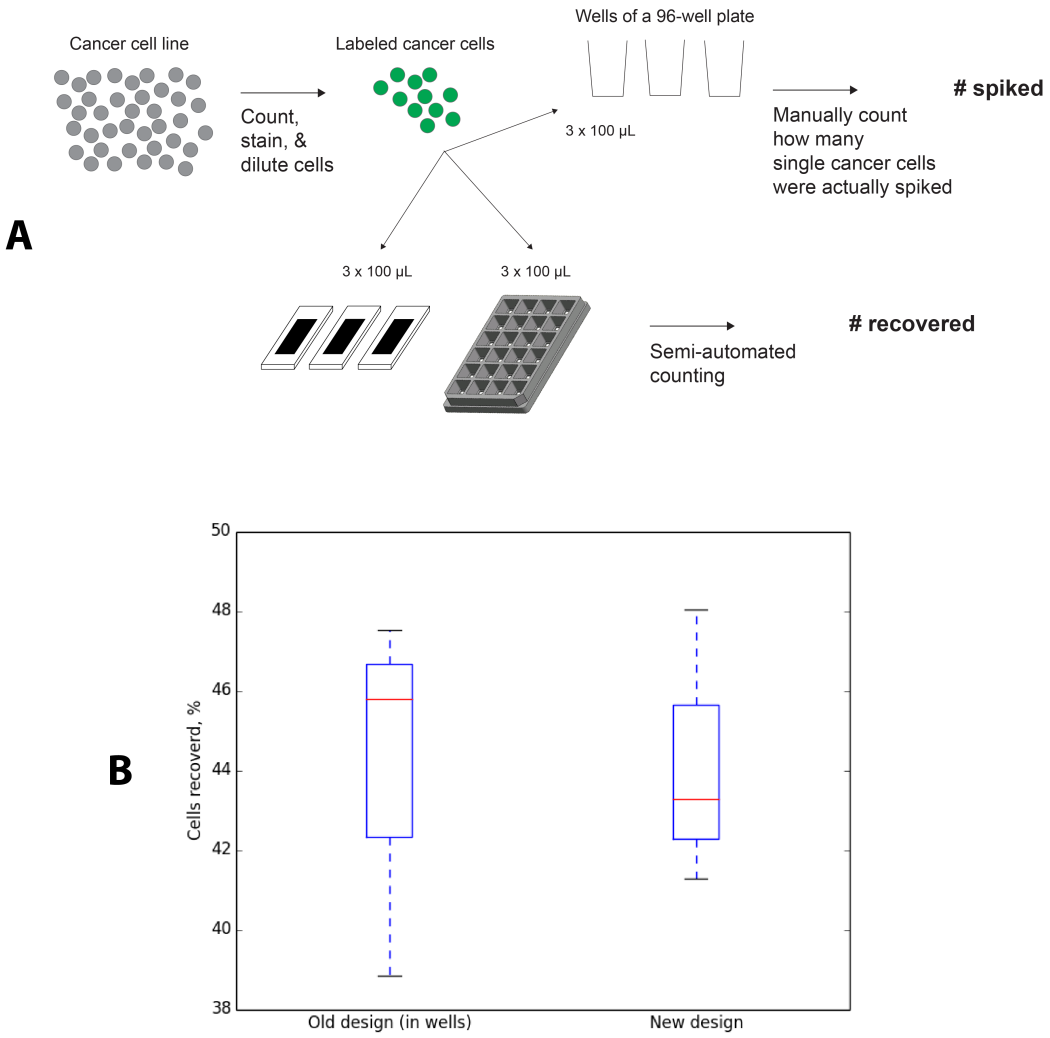

Figure 27. Comparison of cell recovery rates between old and new designs. **(A)** Design of the study. **(B)** Results; whiskers display the range of values (n=3). Figure **(A)** adopted from **Figure 26**b.

3.2.2 Immunophenotyping of small samples.

Robust characterization of human immune responses necessitates measurements that are able to resolve a variety of classes of cells and their unique traits within each class, as well as temporal variations of those traits at the single-cell level [63]. Such fine resolution can only be achieved with special methods designed with high multiplexity in mind. Over the years, polychromatic flow cytometry has proved to be an indispensible tool in this regard [82]. A more recent example, mass cytometry (CyTOF), has allowed for an even greater expansion of the number of simultaneously accessed parameters [83].

These (now becoming orthodox) methods, however, come with a number of inherent limitations. First, due to the inefficiencies in sample processing, the number of cells required to establish a robust statistic with these methods is often far greater ($\sim 10^5$–10^7) than available through standard sample acquisition techniques (small biopsies, cytobrushes, etc.) [84]. Second, traditional methods often destroy viability or lose identity of interrogated cells by the end of analysis, precluding further characterization of these with orthogonal assays; or, while a small subset of cells could be sorted out for further analysis, tracing of many subsets is often desired. As a result, such methods waste precious clinical samples, increasing both patient morbidity and diagnostic costs by requiring multiple sample draws.

Our laboratory has recently developed Multi-Spectral Image Cytometry (MuSIC) that uses a regular epifluorescence microscope to access 16 phenotypic parameters simultaneously on up to 10^5 single cells [84]. The increased spectral resolution is enabled by established methods for compensation between fluorescent channels developed in analogy with polychromatic flow cytometry. Unlike in the latter, however, all cells remain viable and individually accessible for downstream analyses.

One disadvantage of the new method is an increased imaging time spent on each sample (4x or more). We demonstrated the utility of the new nanowell platform for MuSIC by speeding

up image acquisition and analysis compared to regular chips. A standard panel of 15 markers was applied to peripheral blood mononuclear cells (PBMCs) from an individual. These markers allowed us to define populations of T cells (CD45+ CD3+) and other leukocytes (CD45+ CD3-) in this sample (**Figure 28**A, top), and determine several sub-lineages (along with their activation states) among these two (**Figure 28**A, middle and bottom). Further, we applied the same panel to a matched mucosal cytobrush sample from the same individual, and processed both samples on the new and the old arrays (**Figure 28**B). While we observed very similar patterns in cell distributions for each sample across the designs, the distinctions between the two samples were preserved (**Figure 28**B). Further, while we loaded comparable number of cells on both devices, the new format took only a fraction of imaging time required for old arrays (from 1.5 h to ~12 min). This speed-up was enabled by a closer separation between the wells compared to the old platform (10 um versus 50 um) and a smaller border at the edge of the field of view (~25 um versus ~100 um), all of which allowed us to fit many more wells in a block (21 x 21 = 441 compared to 11 x 11 = 121) and decrease the total number of blocks (10 x 10 = 100 versus 15 x 46 = 690), leading to a ~7x decrease in imaging time. In addition, better compartmentalization of samples on the new platform could decrease cross-contamination.

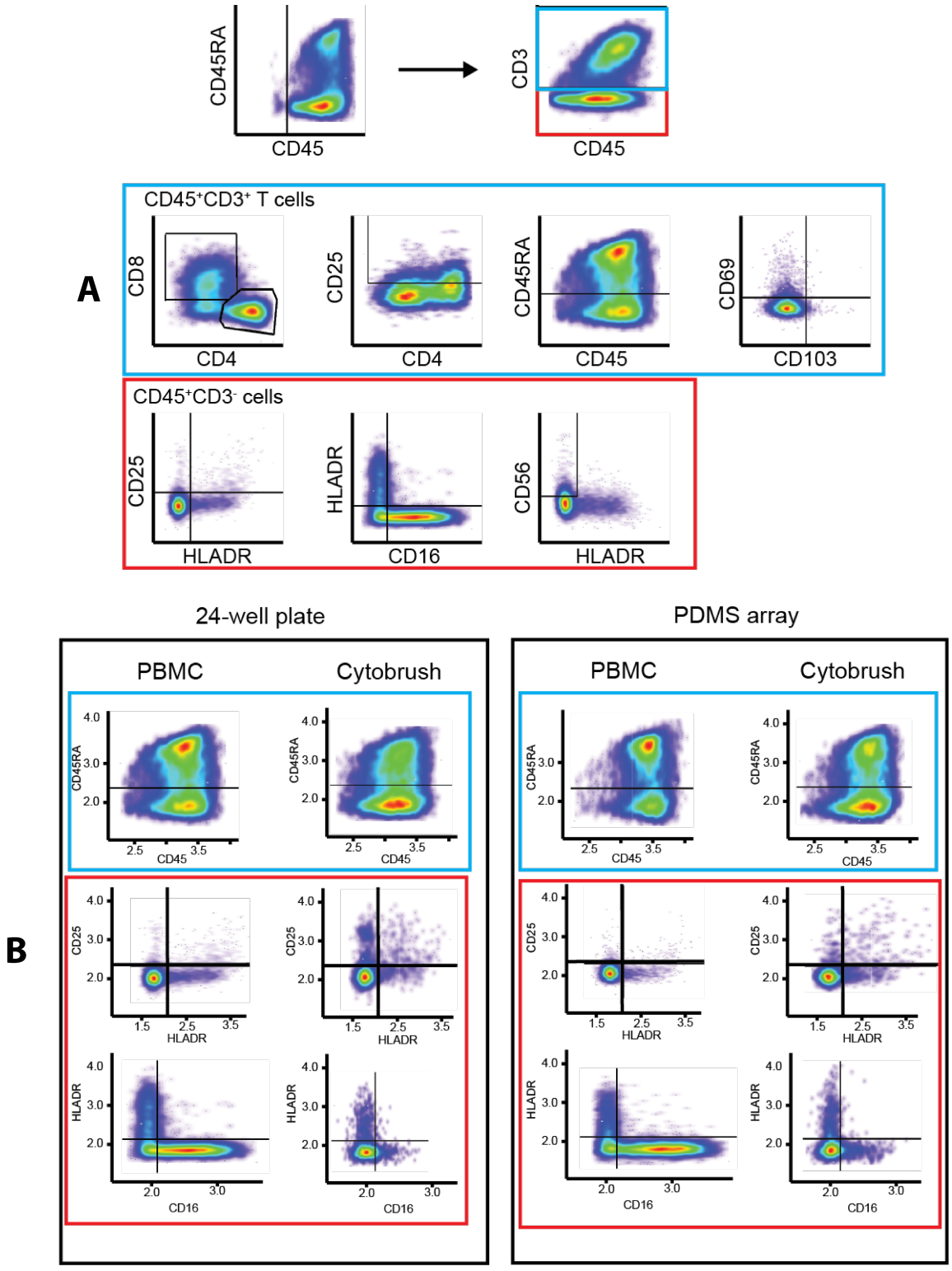

Figure 28. Immunophenotyping with MuSIC. **(A)** Gating of various cell subpopulations from peripheral blood mononuclear cells (PBMCs) imaged on the nanowell plate. **(B)** Comparison of PBMCs and cytobrush samples in the new and the old designs. Figure courtesy Dr. Todd Gierahn.

3.3 Discussion

Here we demonstrated a nanowell plate platform for single-cell analysis as a direct improvement over the established nanowell array format previously developed in our laboratory. The new platform comes in a different form-factor, allowing us to independently process more samples on each device (24 compared to one or a few), greatly cut down times spent on imaging, and directly interface with a range of automated equipment suitable for processing in a standardized format (SBS). Additionally, the new format and associated materials are directly compatible with large-scale replication, a critical limitation of the old arrays.

Although we also expected higher rates of recovery of cells in the new format compared to the old one, the increased throughput of the new design enabled more efficient processing of a greater number of samples, posing a potential for scale-up of single-cell analyses not possible with the previous design. SBS format is the gold standard for automated high-throughput screening assays used in the industry; we have now brought it to phenotypic analyses at the single-cell level that preserve viability, identity, and potential for recovery of cells throughout an experiment. While other SBS-based platforms (such as 96-well plates) may allow for similar types of analyses, we argue that by compartmentalizing cells in the nanowells (a unique feature of our assays), we improve isolation and simplify localization and recovery of individual cells of interest. We demonstrated the utility of our platform in two important examples: enrichment and recovery of circulating tumor cells (rare cells found in the blood of cancer patients and believed to be responsible for metastasis), and immunophenotyping of leukocytes from small tissue or blood samples available on a more regular basis than surgical biopsies. As such, our technology directly addresses the need for analysis and recovery of cells that could be missed or inaccessible through the more established methods of analysis.

One limitation of the new platform is sequential processing of samples. Although the times spent on imaging of each array have drastically decreased compared to the old format, we

still image only one array at a time; multiplied by 24, this leads to a significant total time per each plate (however, it is spent more efficiently). We expect that advances in imaging systems will somewhat alleviate this problem; for example, several cameras simultaneously capturing each field of view (in different channels) would cut the total time proportionately. One could also incorporate several imagers acting in parallel on separate macrowells.

A few other problems could feasibly be solved in the near future. One concern is deficiencies in the automated equipment's interface with our platform (e.g. the arm of our cell picking robot can only reach certain macrowells; this will be addressed with a better manipulator). There are shortcomings in manual gluing of the top and the bottom parts: even under substantial pressure, the glue doesn't spread and cure uniformly, leading to leakage of media from some wells and excessive spread of the glue into the wells; these issues can be efficiently addressed with precise automated spotting of the glue (however, that requires special equipment). There is a non-uniform distortion of blocks from replication of the bottom part (due to uneven heating/cooling and thermal expansion during embossing of the material), which complicates alignment of arrays for imaging and leads to improper shifts in positions of the blocks relative to the grid. The latter problem, together with (perhaps overly small) gaps between the blocks, results in incomplete imaging of some wells at the edges of camera's field of view; this effect can be reduced by allowing more "dead" space between blocks, or with advances in injection molding of small features (albeit at a high cost). Moreover, optical instruments with large fields of view (desirable for high-throughput imaging) suffer from inhomogeneous illumination profile that falls off towards the edges, as illustrated for immunophenotyping in **Figure 29**; this widens distributions of fluorescence intensities for each population of cells, confounding the gating procedure and increasing potential for misclassification. The illumination problem could be addressed by post-processing that accounts for shading, either in software or hardware (as done is some recent cameras), or better still, by improving illumination profile of

the light source. Lastly, retention of cells in the nanowells of the new format is affected by shallow depth of the wells that assists with replication; state-of-the-art methods for DRIE or a combination of DRIE and anisotropic etching may allow increasing the depth while ensuring a positive slant of the walls.

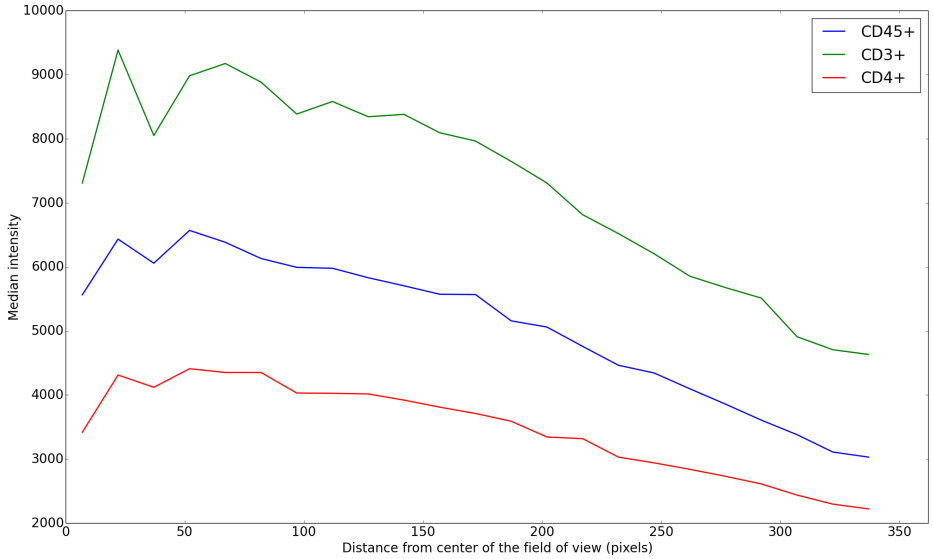

Figure 29. Median intensity across the field of view for several channels.

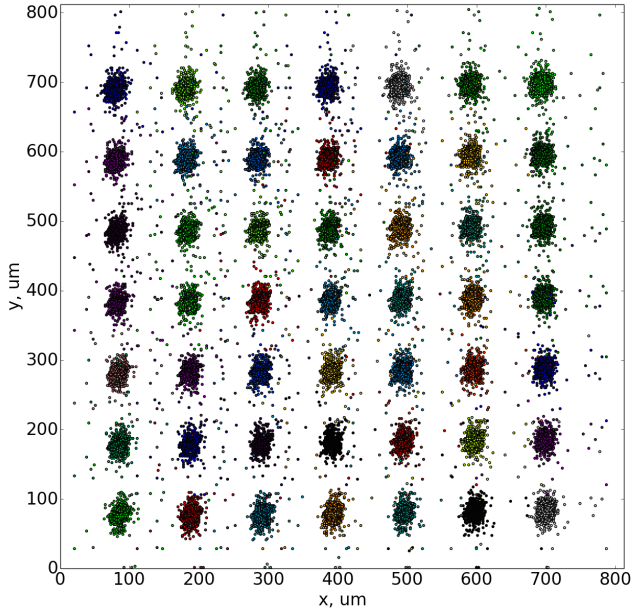

Figure 30. Spread of well centroids across an array (shown for an old chip design).

Finally, the old arrays have been specifically designed for microengraving, which captures elements of the secretome of each cell (in addition to phenotypic traits from cytometry), greatly expanding the amount of information and types of assays available for each cell. Our new format has not yet been interfaced with microengraving, as doing so requires replication of the "printing" procedure wherein the old arrays leveraged the elastic properties of PDMS to conformally seal against a hard surface of the glass slide. Conversely, the new plates are made in a hard material and could thus necessitate the use of a "soft" reciprocal surface. However, elastomeric materials are less amenable to large-scale replication due to long curing times and general "stickiness", although this could be addressed with the newer "thermoplastic elastomers" suitable for extrusion (another potential solution is a hard reciprocal plate with a special relief that fits in the nanowells but doesn't require microscopic alignment). In addition, the raised profile of macrowells leads to a bulky reciprocal format that may be incompatible with specialized microscope slide scanners for reading the fluorescent signal from the "prints"; one solution would be to use high-sensitivity microscopes configured with top-of-the-line components. For example, we could use higher-NA objectives to collect more light; doing so necessitates shorter working distances, but may be enabled by the decreased thickness of the nanowell plates compared to the old PDMS-glass format.

While we have demonstrated the utility of the new platform for analyses of CTCs and mucosal samples, our approach can be applied to any area where identification and recovery of rare cells, or characterization of cellular heterogeneity, are needed, while only small numbers of cells may be available; it could equally apply to stem cells, bacteria and yeast, or highly heterogeneous tumors. Compared to the previous approaches, our platform enables simultaneous high-content and high-throughput phenotypic characterization of single cells, while preserving cell viability and identity for further analyses. Along with standardization of the form-factor, this makes our approach modular enough to be integrated with existing analytical pipelines to enable an even greater degree of characterization of cells and ultimately improve understanding of biological processes and assist diagnostics.

3.4 Methods

Design of masks for the production of masters for the bottom part of nanowell plates was analogous to the process described in Chapter 2. Well arrangement was optimized to fit the field of view of the camera: Hamamatsu ImageEM EM-CCD sensor has 512 x 512 pixels with 16um pixels, and was imaged with 10x, 0.3NA objective (Zeiss) and 0.63x de-magnifying lens. As such, the total field of view was 512 * 16 um / (0.63 * 10) ~ 1300 um wide, imaged at 16 um / 6.3 ~ 2.54 um/pixel; the Abbe diffraction limit at 500 nm is 0.61 * 0.5 um / 0.3 ~ 1um, that is less than the pixel resolution. Each block of wells was then designed to have 21 x 21 of 50 um square wells 10 um separation for a total of (20 * 60 um + 50 um) = 1250 um across, leaving ~ 50 um for the boundary between blocks. Lateral variation in center positions of the blocks (due to imperfect calibration or positioning of the stage) was estimated from previous arrays to be within this value (**Figure 30**).

The upper part with macrowells was designed in Autodesk Inventor 2014 based on official specifications for SBS format [69] and was optimized for draft angles and thicknesses with the help of web-based Protomold ProtoQuote system to be compatible with injection molding. 24-well pattern was chosen to match the arrangement of magnets in MagSweeper, an alternative CTC enrichment device described in [85].

Prototyping of the upper part was initially performed using Stratasys Dimension 1200es 3D printer located at the Laboratory for Engineering Materials (LEM) of the Department of Materials Science and Engineering (DMSE) at MIT. After optimization of dimensions, further prototypes were fabricated in acrylonitrile butadiene styrene (ABS) with stereolithography (SLA) at Quickparts.com Inc.

Masters for the bottom parts were **microfabricated** with anisotropic etching of Si in analogy with the process described in Chapter 2. Alternatively, DRIE of Si wafers was performed at the same facilities (**Figure 22**). Briefly, wafers were treated in HMDS oven, recipe 5 for 15

min. Using Solitec Inc. model 5110 manual photoresist coater, AZ 4620 was dispensed at 1000 rpm for 15 sec and spread at 1500 rpm for 60 sec for ~10 um thickness. After a pre-bake at 95C for 45 min, the photoresist was exposed for 15 sec in EV620 mask aligner (no precision alignment was necessary), developed in AZ 405, and post-baked at 95C for 30 min (lower temperature was required to prevent degradation of this photoresist). Si was then etched with a standard recipe (corresponding to ~1 um/min rate) in a Surface Technology Systems (STS) Inductively Coupled Plasma (ICP) deep trench etching system down to ~20 um depth. Resist was stripped in System One Matrix 106 plasma asher. Additionally, after a piranha clean, C_4F_8 (Teflon) passivation layer could be deposited in the same STS tool to ease up subsequent molding from the master. Finally, the wafers were trimmed to fit the upper part using Disco Abrasive System Model DAD-2H/6T die saw.

Characterization of morphology of the microfabricated masters was performed in secondary electron mode at ~20 kV (since Si is conductive) on JEOL 6010LA general-purpose SEM at the ISN, as its chamber was large enough to accommodate SBS format.

Soft embossing of bottom parts in COP 1430R (or similar COC/COP material) was performed by Edge Embossing LLC from either master with the use of an intermediate elastomeric mold. The upper parts were provided to the same vendor for subsequent gluing to the bottom parts.

The magnetic plate (MagPlate) for CTC enrichment was designed to fit the dimensions of the nanowell plate and was prototyped with the same tools as the upper part (**Figure 31**). Ultra-high pull strength neodymium magnets (McMaster) were glued to the SLA-prototyped plate with Hardman 13230A/B-SY high-peel strength epoxy, same pole down.

Figure 31. Magnetic plate (MagPlate) for CTC enrichment.

Spiking studies for direct **enrichment** of CTCs from blood were carried out as follows. 4 vials of 5mL healthy donor blood (Research Blood Components) were each mixed with 50 mL of 1x Pharm Lyse (BD Biosciences) and incubated at RT for 15 min. Lysed blood was then spun at 200g for 5 min at 4C. After removal of supernatant, each leukocyte pellet was resuspended in 400 uL of HBSS. 450 uL of each suspension was then combined with others, and the total volume was brought to 2000 uL; this volume represented all PBMCs from the initial 20 mL of blood, as could be confirmed by counting. LNCaP cells (ATCC), while adhered as grown, were stained with 1:1000 Calcein AM in media (DMEM + 10% FBS) at 37C for 15 min, washed with 1 mL of Hank's Balanced Salt Solution (HBSS), trypsinized and resuspended in media to ~1700 cells/mL. 50 uL of this suspension was imaged in FITC channel on Zeiss AxioObserver Z1; the images were stitched, and cells were counted. Alternatively, 50 uL of this suspension (containing an estimated equal number of cells) was spiked into each of 100, 100, 500 and 1000 uL of PBMC

suspension described above to represent 1, 1, 5 and 10 mL of RBC-lysed blood containing CTCs. Each sample was incubated with 2 uL of CELLection Epithelial Enrich Dynabeads (Life Technologies) on a tube rotator at 4C for 30 min, and then with 15 uL of Alexa647-anti-CD45 and 15 uL of PECy7-anti-EpCAM for another 20 min. Nanowell plates were covered with Microseal 'B' Adhesive Seal (Bio-Rad), and small holes were poked in the film above all macrowells to prevent popping in the vacuum chamber of the plasma cleaner during the next step; the film above wells to be used was cut out. After plasma-treatment of wells for 5 min, 1 mL of 1:10 10x PBS : Percoll (GE Life Sciences) was loaded in each of 4 macrowells, and 1 mL of each sample from above was gently layered on top of respective wells. The beads (with or without LNCaPs) were allowed to settle for 15 min by gravity and then put on MagPlate at RT for another 10 min (if put on the magnets immediately, beads pulled a lot of WBCs with them as well). Cells were then imaged on Axio Observer Z1 in DAPI, FITC, PE/Cy7 and 647 channels and manually counted from the resultant images (for better accuracy), using Enumerator for visualization. To estimate time required for settling by gravity, time-lapse experiments were set up over a period of 2 h, and later visualized as movies; most beads (with or without cells) were observed to settle (i.e. travel the full thickness of Percoll) within ~50 min (**Figure 32**). However, once the beads and bead-cell conjugates propagated into the upper layer of Percoll, they could be pulled with the magnet to speed up settling times while avoiding pulling any WBCs with them.

For comparison of cell **recovery** rates between SBS format nanowells and an old chip design (10 x 10 blocks of 21 x 21 wells – 100 positions and 44100 wells in total, compared to 72 x 24 blocks of 7 x 7 wells – 1728 positions and 84672 wells in total), we loaded 100 uL of fixed LNCaP cells stained with CellSearch Epithelial Cell Kit (Janssen Diagnostics) at ~15000 cells/mL on each array, along with wells of a 96-well plate, in replicates of 3 (**Figure 27**a). Cells in the 96-well plate were counted manually for better accuracy; to simulate a real-case scenario, cells on arrays were identified and counted with a semi-automated ImageJ-based processing routine, while well locations were defined by Enumerator. The recovery rates from arrays relative

to counts from the 96-well plate are shown in **Figure 27**b.

Immunophenotyping experiments were set up for both the new and the old design by Dr. Todd Gierahn (MIT) as described in [84].

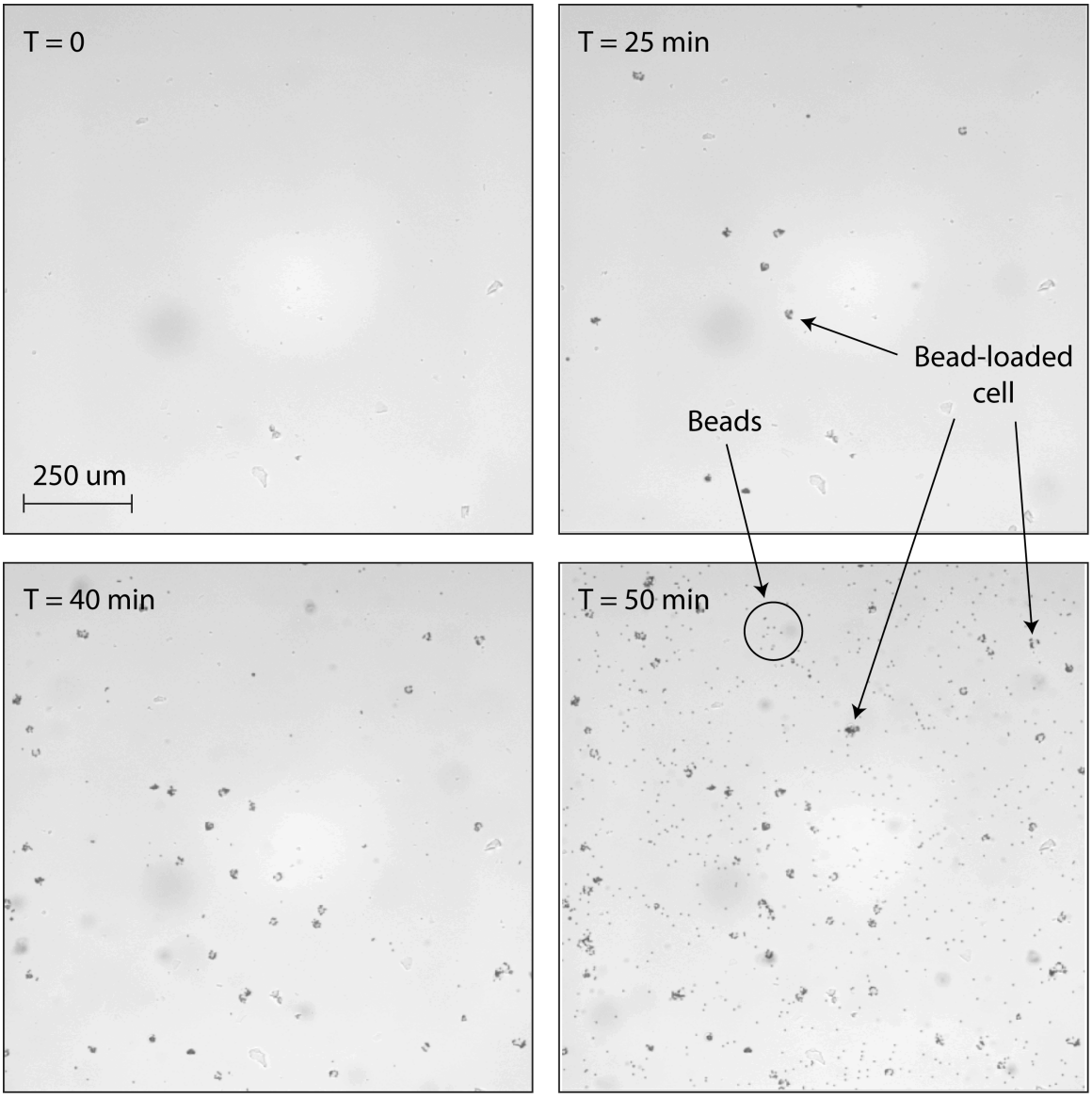

Figure 32. Process of gravity-based settling of cells loaded with beads through the layer of Percoll.

4. Conclusion

4.1 Summary

Single-cell analysis is a burgeoning field of research that studies characteristics of individual cells in a given population. Traditional methods in molecular biology determine only an "average" behavior, masking contributions coming from the individual players. Many important areas concerning human health, such as immunology and cancer biology, deal with highly heterogeneous populations where these contributions cannot be ignored.

Here we developed two methods of analysis to resolve this heterogeneity and uncover characteristics of individual cells. Building on advances in microfabrication over the last decades, we have implemented arrays of microscopic wells to isolate and interrogate single cells, while preserving their identity and possibility of integration of several types of analysis. We have also demonstrated the utility of these arrays for potential clinical applications.

The first platform complements fluorescence-based cytometry with a label-free method of detection of small molecules, such as lipids and metabolites, relying on MALDI mass spectrometry. We first sought to use an existing PDMS-based array to isolate and image many individual cells and then transfer them in parallel to a conductive substrate required for MALDI. Although we had partial success with this procedure, even with "release" coatings the rates of transfer were suboptimal, and the registration pattern of cells was lost. To facilitate imaging of cells directly on a chip, we produced a hard plastic array of microwells with a semi-transparent conductive coating. This device demonstrated degraded MALDI signal that we attributed to poor sidewall coverage in the wells, as well as possible ablation of the plastic material and its outgassing in the instrument. We finally fabricated microwell arrays with anisotropic etching of Si, which (after coating with a conductive layer) provided an adequate substrate for MALDI and allowed us to proceed with further analysis. To increase sensitivity of the technique, we also used an in-house matrix sublimation apparatus for sample preparation. To relate the acquired mass

spectrometric and fluorescence signals for every cell, we developed a registration procedure relying on the precise geometry of the chip and its compound image from a microscope. Finally, we detected phospholipid signatures of two cancer cell lines, as well as a change in the phospholipid profile of one of them in response to a lipid kinase inhibitor.

The second platform is an improvement over the existing PDMS-based microwell (here referred to as "nanowell") arrays for phenotypic analysis of single cells. We sought to standardize the nanowell array format to provide compatibility with the automated equipment designed for use with the SBS plate form-factor, as well as to expand the number of samples independently processed on each device and increase the efficiency in image acquisition for each sample. We fabricated prototypes of the nanowell plates with two matching pieces: a macrowell plate for compartmentalization of samples, and a grid of nanowell arrays for isolation, interrogation and recovery of individual cells. Each part was fabricated with materials and methods most suited for the replication of its features at their characteristic scale. We applied the new plates to the analysis of rare circulating tumor cells (CTCs) found in the blood of metastatic patients. We also developed an on-chip density-assisted immunomagnetic method for enrichment of these cells. The new platform demonstrated high rates of recovery of CTCs that were comparable to the old platform but considerably more efficient with regards to imaging and analysis. The new plates also proved useful for high-content immunophenotyping of leukocytes from small mucosal and blood samples. We applied previously developed multi-spectral image cytometry (MuSIC) to the analysis of these samples and demonstrated a much-improved efficiency in sample processing.

The main advantages of these platforms over the more traditional single-cell analysis tools such as polychromatic flow cytometry and (more recently) CyTOF, are modularity and overall simplicity, as well as potential for processing of small clinical samples. While regular tools often lose track of individual cells in the course of analysis and require substantial numbers of cells not readily found in limited clinical samples, our approach allows to identify and analyze single cells and their responses to uniformly applied perturbations from small (epi-)genetically

heterogeneous populations. We can also preserve viability and recover individual cells when using a fluorescence-only pipeline, or obtain the lipid or metabolic profile of each cell as an end-point assay that, unlike CyTOF, doesn't involve the need for expensive isotope tags, and may potentially be universally extended to other types of molecules. Finally, our approach could be valuable for studying interactions between multiple cells per well in a more direct way than in flow cytometry [2].

4.2 Perspectives

Despite the advantages described above, the current iterations of our platforms have a number of limitations. For MALDI analysis, we used a non-transparent material (Si) that confounds image-guided processing and analysis of cells. This problem can be solved with the development of a glass-based backend for the microwells, but requires a more involved process that increases the cost of production. In addition, current devices are not reusable, which also affects their cost; we could tweak the fabrication process (e.g. switch the gold coating for a highly-doped surface layer in Si) to make them compatible with piranha cleaning protocol. Another issue is inherently low sensitivity of the MALDI instruments that limits detection to only the most abundant molecules; we can reasonably expect an improvement in this direction with better instruments in the future.

Despite our expectation that the rates of recovery of cells with the old chip design would be substantially lower than with densely packed wells in the new plates, they proved to be similar. This observation suggests that nanowells by themselves are very effective at isolating individual cells from suspension; as such, density of wells does not necessarily relate to rates of recovery. However, the same amount of cells could be processed on a smaller area of the chip the closer the wells are, thus improving overall efficiency in sample processing. We could also help retain more cells in the wells if we made them deeper. Unfortunately, increasing the aspect ratio of

microscopic features is not always feasible from the fabrication point of view. For processes relying on molding, taller posts on the master increase the area of contact with the substrate, which complicates unmolding due to additional friction; they may also deform if the process involves an elastomeric master. In photolithographic processes for the production of masters or devices (such as those relying on SU-8), greater thicknesses lead to less uniform photoresist coatings and prolong development times, which may also lead to feature distortion. Nevertheless, optimization of sizes of wells to increase the efficiency of loading of single cells is possible [6], whereas stochastic loading may be beneficial for studying cell interactions. One could also prevent cell migration from the wells while preserving cell viability by sealing the array with a semi-permeable membrane; unlike for actively actuated microfluidic perfusion systems, this approach would not substantially increase the complexity of our assays, although it would require the use of a limited number of biocompatible chemistries.

We also anticipate integration of our platform with the microengraving process. As discussed in more detail in Chapter 3, this would substantially improve the utility of our assays, but most likely necessitate the development of a soft reciprocal surface and a variation in the geometry of the plates. For instance, we could envision a modular device resembling a printing press that would be assembled for compartmentalization of samples and microengraving and later "released" to separately scan individual arrays and their imprints. Large-scale production of these devices could ultimately be achieved with injection molding; we intentionally omitted a discussion of this method due to its high costs that extend beyond the capacities of an academic lab. Alternatively, one could fabricate microwell arrays in a photocurable elastomer patterned on glass; one of the most promising commercial rapid microproduct development (RPMD) technologies for this purpose is available from microTEC GmbH [86]. This approach could also incorporate ITO-coated glass substrates for MALDI, although its compatibility with laser ablation remains to be confirmed.

We also omitted the more advanced downstream steps in single cell analysis, including

picking of individual cells and whole-genome or whole-exome sequencing (WGS/WES) [76]. Manipulation of single cells is a nontrivial process often performed manually with a micropipette or using dedicated automated precision instruments [81]. Scarce availability and associated cost of the latter poses an ultimate limit on the throughput of any analytical pipeline that involves transfer of individual cells; further improvements in this direction will clearly be required. WES is another involved process that follows many preparatory steps that could easily be affected by an operator error; further improvement of its pipeline will require automation of individual steps and development of information handling systems. Another bottleneck area is image analysis; reliable identification of cells of interest in a high-throughput manner will necessitate the use of advanced image processing and pattern recognition algorithms, perhaps involving machine-learning techniques to reduce human participation.

Ultimately, we would like to free up the researcher as much as possible from mundane steps prone to the human error, and allow them to focus on more complicated tasks such as data interpretation. The ability to effortlessly and inexpensively gather and integrate meaningful high-content datasets at the single-cell level will provide invaluable insights into human clinical research. This will facilitate the transition from exploratory biology involving “averages” and generalized principles to a more personalized approach tailored to the diagnosis and treatment of each individual patient.

References

[1] D. Di Carlo, H. T. K. Tse, and D. R. Gossett, "Introduction: Why Analyze Single Cells?," in *Methods in Molecular Biology*, vol. 853, no. 1, Humana Press, 2012, pp. 1–10.

[2] A. Yalçın, Y. J. Yamanaka, and J. C. Love, "Analytical Technologies for Integrated Single-Cell Analysis of Human Immune Responses," in *Methods in Molecular Biology*, vol. 853, no. 16, Totowa, NJ: Humana Press, 2012, pp. 211–235.

[3] Dino Di Carlo, A. Nima Aghdam, and L. P. Lee, "Single-Cell Enzyme Concentrations, Kinetics, and Inhibition Analysis Using High-Density Hydrodynamic Cell Isolation Arrays," *Anal. Chem.*, vol. 78, no. 14, pp. 4925–4930, May 2006.

[4] R. J. Taylor, D. Falconnet, A. Niemistö, S. A. Ramsey, S. Prinz, I. Shmulevich, T. Galitski, and C. L. Hansen, "Dynamic analysis of MAPK signaling using a high-throughput microfluidic single-cell imaging platform," *PNAS*, vol. 106, no. 10, pp. 3758–3763, Mar. 2009.

[5] J. F. Edd, D. Di Carlo, K. J. Humphry, S. Köster, D. Irimia, D. A. Weitz, and M. Toner, "Controlled encapsulation of single-cells into monodisperse picolitre drops," *Lab Chip*, vol. 8, no. 8, pp. 1262–1264, 2008.

[6] J. R. Rettig and A. Folch, "Large-Scale Single-Cell Trapping And Imaging Using Microwell Arrays," *Anal. Chem.*, vol. 77, no. 17, pp. 5628–5634, Sep. 2005.

[7] S. Kobel, A. Valero, J. Latt, P. Renaud, and M. Lutolf, "Optimization of microfluidic single cell trapping for long-term on-chip culture," *Lab Chip*, vol. 10, no. 7, pp. 857–863, 2010.

[8] E. Brouzes, M. Medkova, N. Savenelli, D. Marran, M. Twardowski, J. B. Hutchison, J. M. Rothberg, D. R. Link, N. Perrimon, and M. L. Samuels, "Droplet microfluidic technology for single-cell high-throughput screening," *PNAS*, vol. 106, no. 34, pp. 14195–14200, Aug. 2009.

[9] J. J. Agresti, E. Antipov, A. R. Abate, K. Ahn, A. C. Rowat, J.-C. Baret, M. Marquez, A. M. Klibanov, A. D. Griffiths, and D. A. Weitz, "Ultrahigh-throughput screening in drop-based microfluidics for directed evolution," *PNAS*, vol. 107, no. 9, pp. 4004–4009, Mar. 2010.

[10] J.-C. Baret, O. J. Miller, V. Taly, M. Ryckelynck, A. El-Harrak, L. Frenz, C. Rick, M. L. Samuels, J. B. Hutchison, J. J. Agresti, D. R. Link, D. A. Weitz, and A. D. Griffiths, "Fluorescence-activated droplet sorting (FADS): efficient microfluidic cell sorting based on enzymatic activity," *Lab Chip*, vol. 9, no. 13, pp. 1850–1858, 2009.

[11] M. Chabert and J.-L. Viovy, "Microfluidic high-throughput encapsulation and hydrodynamic self-sorting of single cells," *PNAS*, vol. 105, no. 9, pp. 3191–3196, Mar. 2008.

[12] A. Revzin, K. Sekine, A. Sin, R. G. Tompkins, and M. Toner, "Development of a microfabricated cytometry platform for characterization and sorting of individual leukocytes," *Lab Chip*, vol. 5, no. 1, pp. 30–37, 2005.

[13] J. C. Love, J. L. Ronan, G. M. Grotenbreg, A. G. van der Veen, and H. L. Ploegh, "A microengraving method for rapid selection of single cells producing antigen-specific antibodies," *Nat. Biotechnol.*, vol. 24, no. 6, pp. 703–707, May 2006.

[14] J. C. McDonald and G. M. Whitesides, "Poly(dimethylsiloxane) as a Material for Fabricating Microfluidic Devices," *Acc. Chem. Res.*, vol. 35, no. 7, pp. 491–499, Jul. 2002.

[15] R. Mukhopadhyay, "When PDMS isn't the best," *Anal. Chem.*, vol. 79, no. 9, pp. 3248–3253, May 2007.

[16] Y. Xia, "Soft lithography," *Annu. Rev. Mater. Sci.*, vol. 28, pp. 153–184, 1998.

[17] P. S. Nunes, P. D. Ohlsson, O. Ordeig, and J. P. Kutter, “Cyclic olefin polymers: emerging materials for lab-on-a-chip applications,” *Microfluid Nanofluid*, vol. 9, no. 2, pp. 145–161, Aug. 2010.

[18] D. N. Louis, H. Ohgaki, O. D. Wiestler, W. K. Cavenee, P. C. Burger, A. Jouvet, B. W. Scheithauer, and P. Kleihues, “The 2007 WHO Classification of Tumours of the Central Nervous System,” *Acta Neuropathol*, vol. 114, no. 2, pp. 97–109, Sep. 2007.

[19] L. S. Eberlin, I. Norton, A. L. Dill, A. J. Golby, K. L. Ligon, S. Santagata, R. G. Cooks, and N. Y. R. Agar, “Classifying human brain tumors by lipid imaging with mass spectrometry.,” vol. 72, no. 3, pp. 645–654, Feb. 2012.

[20] F. B. Furnari, T. Fenton, R. M. Bachoo, A. Mukasa, J. M. Stommel, A. Stegh, W. C. Hahn, K. L. Ligon, D. N. Louis, C. Brennan, L. Chin, R. A. DePinho, and W. K. Cavenee, “Malignant astrocytic glioma: genetics, biology, and paths to treatment,” *Genes Dev.*, vol. 21, no. 21, pp. 2683–2710, Nov. 2007.

[21] J. M. Francis, C.-Z. Zhang, C. L. Maire, J. Jung, V. E. Manzo, V. A. Adalsteinsson, H. Homer, S. Haidar, B. Blumenstiel, C. S. Pedamallu, A. H. Ligon, J. C. Love, M. Meyerson, and K. L. Ligon, “EGFR variant heterogeneity in glioblastoma resolved through single-nucleus sequencing,” *Cancer Discov.*, vol. 4, no. 8, pp. 956–971, Jun. 2014.

[22] B. Pang, W. Wan, C. Lee, K. J. Khu, and W. Ng, “The role of surgery in high-grade glioma - Is surgical resection justified? A review of the current knowledge,” *Ann. Acad. Med. Singapore*, vol. 36, no. 5, pp. 358–363, 2007.

[23] N. Y. Agar, A. J. Golby, K. L. Ligon, I. Norton, V. Mohan, J. M. Wiseman, A. Tannenbaum, and F. A. Jolesz, “Development of stereotactic mass spectrometry for brain tumor surgery,” *Neurosurgery*, vol. 68, no. 2, pp. 280–290, Feb. 2011.

[24] S. A. Schwartz, R. J. Weil, R. C. Thompson, Y. Shyr, J. H. Moore, S. A. Toms, M. D. Johnson, and R. M. Caprioli, “Proteomic-based prognosis of brain tumor patients using direct-tissue matrix-assisted laser desorption ionization mass spectrometry,” *Cancer Res.*, vol. 65, no. 17, pp. 7674–7681, 2005.

[25] J. C. Jurchen, S. S. Rubakhin, and J. V. Sweedler, “MALDI-MS imaging of features smaller than the size of the laser beam,” *J Am Soc Mass Spectrom*, vol. 16, no. 10, pp. 1654–1659, Oct. 2005.

[26] B. Keller, “Detection of 25,000 molecules of substance P by MALDI-TOF mass spectrometry and investigations into the fundamental limits of detection in MALDI,” *J Am Soc Mass Spectrom*, vol. 12, no. 9, pp. 1055–1063, 2001.

[27] R Lemaire, M Wisztorski, A Desmons, J C Tabet, R Day, A. M Salzet, I Fournier, “MALDI-MS Direct Tissue Analysis of Proteins: Improving Signal Sensitivity Using Organic Treatments,” *Anal. Chem.*, vol. 78, no. 20, pp. 7145–7153, Sep. 2006.

[28] E. H. Seeley, S. R. Oppenheimer, D. Mi, P. Chaurand, and R. M. Caprioli, “Enhancement of protein sensitivity for MALDI imaging mass spectrometry after chemical treatment of tissue sections,” *J Am Soc Mass Spectrom*, vol. 19, no. 8, pp. 1069–1077, Aug. 2008.

[29] Y. Schober, S. Guenther, B. Spengler, and A. Römpp, “Single Cell Matrix-Assisted Laser Desorption/Ionization Mass Spectrometry Imaging,” *Anal. Chem.*, vol. 84, no. 15, pp. 6293–6297, 2012.

[30] A. El-Aneed, A. Cohen, and J. Banoub, “Mass Spectrometry, Review of the Basics: Electrospray, MALDI, and Commonly Used Mass Analyzers,” *Applied Spectroscopy Reviews*, vol. 44, no. 3, pp. 210–230, Apr. 2009.

[31] S. A. Schwartz, M. L. Reyzer, and R. M. Caprioli, “Direct tissue analysis using matrix-assisted laser desorption/ionization mass spectrometry: practical aspects of sample preparation,” *J. Mass Spectrom.*, vol. 38, no. 7, pp. 699–708, 2003.

[32] R. Kruse and J. V. Sweedler, “Spatial profiling invertebrate ganglia using MALDI MS,”

J Am Soc Mass Spectrom, vol. 14, no. 7, pp. 752–759, Jul. 2003.

[33] A. J. Sloane, J. L. Duff, N. L. Wilson, P. S. Gandhi, C. J. Hill, F. G. Hopwood, P. E. Smith, M. L. Thomas, R. A. Cole, N. H. Packer, E. J. Breen, P. W. Cooley, D. B. Wallace, K. L. Williams, and A. A. Gooley, "High Throughput Peptide Mass Fingerprinting and Protein Macroarray Analysis Using Chemical Printing Strategies," *Molecular & Cellular Proteomics*, vol. 1, no. 7, pp. 490–499, Jul. 2002.

[34] Hans-Rudolf Aerni, A. Dale S Cornett, and R. M. Caprioli, "Automated Acoustic Matrix Deposition for MALDI Sample Preparation," *Anal. Chem.*, vol. 78, no. 3, pp. 827–834, 2005.

[35] N. Y. R. Agar, J.-M. Kowalski, P. J. Kowalski, J. H. Wong, and J. N. Agar, "Tissue Preparation for the In Situ MALDI MS Imaging of Proteins, Lipids, and Small Molecules at Cellular Resolution," in *Methods in Molecular Biology*, vol. 656, no. 24, Humana Press, 2010, pp. 415–431.

[36] W. Bouschen, O. Schulz, D. Eikel, and B. Spengler, "Matrix vapor deposition/recrystallization and dedicated spray preparation for high‐resolution scanning microprobe matrix‐assisted laser desorption/ionization imaging mass spectrometry (SMALDI‐MS) of tissue and single cells," *Rapid Commun. Mass Spectrom.*, vol. 24, no. 3, pp. 355–364, 2010.

[37] J. Yang and R. M. Caprioli, "Matrix Sublimation/Recrystallization for Imaging Proteins by Mass Spectrometry at High Spatial Resolution," *Anal. Chem.*, vol. 83, no. 14, pp. 5728–5734, Jul. 2011.

[38] Yuki Sugiura, A. Shuichi Shimma, Mitsutoshi Setou, "Two-step matrix application technique to improve ionization efficiency for matrix-assisted laser desorption/ionization in imaging mass spectrometry," *Anal. Chem.*, vol. 78, no. 24, pp. 8227–8235, Dec. 2006.

[39] K. J. Boggio, E. Obasuyi, K. Sugino, S. B. Nelson, N. Y. Agar, and J. N. Agar, "Recent advances in single-cell MALDI mass spectrometry imaging and potential clinical impact," *Expert Rev Proteomics*, vol. 8, no. 5, pp. 591–604, Oct. 2011.

[40] E. B. Monroe, Eric B Monroe, J. C. Jurchen, John C Jurchen, B. A. Koszczuk, Beth Anne Koszczuk, J. L. Losh, Jenna L Losh, A. Stanislav S Rubakhin, Jonathan V Sweedler, "Massively Parallel Sample Preparation for the MALDI MS Analyses of Tissues," *Anal. Chem.*, vol. 78, no. 19, pp. 6826–6832, Aug. 2006.

[41] M. Schuerenberg, C. Luebbert, H. Eickhoff, M. Kalkum, H. Lehrach, and E. Nordhoff, "Prestructured MALDI-MS sample supports," *Anal. Chem.*, vol. 72, no. 15, pp. 3436–3442, Aug. 2000.

[42] S. Jespersen, W. M. A. Niessen, U. R. Tjaden, J. van der Greef, E. Litborn, U. Lindberg, J. Roeraade, and F. Hillenkamp, "Attomole detection of proteins by matrix-assisted laser desorption/ionization mass spectrometry with the use of picolitre vials," *Rapid Commun. Mass Spectrom.*, vol. 8, no. 8, pp. 581–584, Aug. 1994.

[43] A. O. Ogunniyi, C. M. Story, E. Papa, E. Guillen, and J. C. Love, "Screening individual hybridomas by microengraving to discover monoclonal antibodies," *Nat Protoc*, vol. 4, no. 5, pp. 767–782, Apr. 2009.

[44] M. Glückmann and M. Karas, "The initial ion velocity and its dependence on matrix, analyte and preparation method in ultraviolet matrix‐assisted laser desorption/ionization," *J. Mass Spectrom.*, vol. 34, no. 5, pp. 467–477, May 1999.

[45] P. Chaurand, S. A. Schwartz, D. Billheimer, B. J. Xu, A. Crecelius, and R. M. Caprioli, "Integrating Histology and Imaging Mass Spectrometry," *Anal. Chem.*, vol. 76, no. 4, pp. 1145–1155, Feb. 2004.

[46] T. J. Garrett, M. C. Prieto-Conaway, and V. Kovtoun, "Imaging of small molecules in tissue sections with a new intermediate-pressure MALDI linear ion trap mass spectrometer," *Int J Mass Spectrom*, vol. 260, no. 2, pp. 166–176, 2007.

[47] M. L. Easterling, T. H. Mize, and I. J. Amster, "Routine Part-per-Million Mass Accuracy for High- Mass Ions: Space-Charge Effects in MALDI FT-ICR," *Anal. Chem.*, vol. 71, no. 3, pp. 624–632, Feb. 1999.

[48] H. Kim, C. M. Gilmore, A. Piqué, J. S. Horwitz, H. Mattoussi, H. Murata, Z. H. Kafafi, and D. B. Chrisey, "Electrical, optical, and structural properties of indium–tin–oxide thin films for organic light-emitting devices," *J. Appl. Phys.*, vol. 86, no. 11, pp. 6451–6461, 1999.

[49] T. Minami, "Present status of transparent conducting oxide thin-film development for Indium-Tin-Oxide (ITO) substitutes," *Thin Solid Films*, vol. 516, no. 17, pp. 5822–5828, 2008.

[50] M. Morra, E. Occhiello, R. Marola, F. Garbassi, P. Humphrey, and D. Johnson, "On the aging of oxygen plasma-treated polydimethylsiloxane surfaces," *J. Colloid Interface Sci.*, vol. 137, no. 1, pp. 11–24, Jun. 1990.

[51] T. Kaufmann and B. J. Ravoo, "Stamps, inks and substrates: polymers in microcontact printing," *Polym. Chem.*, vol. 1, no. 4, p. 371, 2010.

[52] J. Narasimhan and I. Papautsky, "Polymer embossing tools for rapid prototyping of plastic microfluidic devices," *J. Micromech. Microeng.*, vol. 14, no. 1, pp. 96–103, Oct. 2003.

[53] K. Dreisewerd, "The desorption process in MALDI," *Chem. Rev.*, vol. 103, no. 2, pp. 395–425, 2003.

[54] S. Lazare and V. Granier, "Ultraviolet laser photoablation of polymers: a review and recent results," *Laser Chem*, vol. 10, no. 1, pp. 25–40, 1989.

[55] A. D. Rakic, A. B. Djurišic, J. M. Elazar, and M. L. Majewski, "Optical Properties of Metallic Films for Vertical-Cavity Optoelectronic Devices," *Appl. Opt.*, vol. 37, no. 22, pp. 5271–5283, 1998.

[56] H. Seidel, "Anisotropic Etching of Crystalline Silicon in Alkaline Solutions: I. Orientation Dependence and Behavior of Passivation Layers," *J. Electrochem. Soc.*, vol. 137, no. 11, pp. 3612–3626, 1990.

[57] X. Liu, J. L. Ide, I. Norton, M. A. Marchionni, M. C. Ebling, L. Y. Wang, E. Davis, C. M. Sauvageot, S. Kesari, K. A. Kellersberger, M. L. Easterling, S. Santagata, D. D. Stuart, J. Alberta, J. N. Agar, C. D. Stiles, and N. Y. R. Agar, "Molecular imaging of drug transit through the blood-brain barrier with MALDI mass spectrometry imaging," *Sci. Rep.*, vol. 3, Oct. 2013.

[58] S. Lindström, R. Larsson, and H. Andersson-Svahn, "Towards high-throughput single cell/clone cultivation and analysis," *Electrophoresis*, vol. 29, no. 6, pp. 1219–1227, 2008.

[59] K. Saraswat, "Metal/Semiconductor Ohmic Contacts," *http://web.stanford.edu/class/ee311/NOTES/Contacts.pdf*.

[60] J. D. Plummer, *Silicon VLSI technology: fundamentals, practice, and modeling*. Pearson Education, 2001.

[61] H. Seidel, "Anisotropic Etching of Crystalline Silicon in Alkaline Solutions: II. Influence of Dopants," *J. Electrochem. Soc.*, vol. 137, no. 11, pp. 3626–3632, 1990.

[62] *DXF Reference*. Autodesk, Inc., 2007.

[63] P. K. Chattopadhyay, T. M. Gierahn, M. Roederer, and J. C. Love, "Single-cell technologies for monitoring immune systems," *Nat Immunol*, vol. 15, no. 2, pp. 128–135, Jan. 2014.

[64] V. Panagiotou, K. R. Love, B. Jiang, J. Nett, T. Stadheim, and J. C. Love, "Generation and Screening of Pichia pastoris Strains with Enhanced Protein Production by Use of Microengraving," vol. 77, no. 9, pp. 3154–3156, Apr. 2011.

[65] C. Alix-Panabières and K. Pantel, "Technologies for detection of circulating tumor cells: facts and vision," *Lab Chip*, vol. 14, no. 1, pp. 57–62, 2014.

[66] L. A. Herzenberg, D. Parks, B. Sahaf, O. Perez, M. Roederer, and L. A. Herzenberg, "The History and Future of the Fluorescence Activated Cell Sorter and Flow Cytometry: A View from Stanford," *Clin Chem.*, vol. 48, no. 10, pp. 1819–1827, 2002.

[67] "Publications from Fluidigm single-cell genomics customers," *http://www.fluidigm.com/home/fluidigm/docs/bib-customer-papers-a1.pdf*.

[68] S. Lindström and H. Andersson-Svahn, "Miniaturization of biological assays — Overview on microwell devices for single-cell analyses," *Biochim. Biophys. Acta*, vol. 1810, no. 3, pp. 308–316, Mar. 2011.

[69] "SLAS Microplate Standards," *http://www.slas.org/resources/information/industry-standards/*.

[70] C. K. Chua, K. F. Leong, and C. S. Lim, *Rapid Prototyping: Principles and Applications*, 3rd ed. World Scientific, 2010.

[71] K.-S. Chen, A. A. Ayón, X. Zhang, and S. M. Spearing, "Effect of process parameters on the surface morphology and mechanical performance of silicon structures after deep reactive ion etching (DRIE)," *J. Microelectromech. Syst.*, vol. 11, no. 3, pp. 264–275, Jun. 2002.

[72] V. A. Adalsteinsson and J. C. Love, "Toward engineered processes for sequencing-based analysis of single circulating tumor cells," *Current opinion in chemical engineering*, vol. 4, pp. 97–104, 2014.

[73] W. J. Allard, J. Matera, M. C. Miller, M. Repollet, M. C. Connelly, C. Rao, A. G. J. Tibbe, J. W. Uhr, and L. W. M. M. Terstappen, "Tumor cells circulate in the peripheral blood of all major carcinomas but not in healthy subjects or patients with nonmalignant diseases," *Clin Cancer Res*, vol. 10, no. 20, pp. 6897–6904, Oct. 2004.

[74] C. Alix-Panabières, H. Schwarzenbach, and K. Pantel, "Circulating Tumor Cells and Circulating Tumor DNA," *Annu. Rev. Med.*, vol. 63, no. 1, pp. 199–215, Feb. 2012.

[75] C. Alix-Panabières and K. Pantel, "Circulating tumor cells: liquid biopsy of cancer," *Clin Chem.*, vol. 59, no. 1, pp. 110–118, Jan. 2013.

[76] J. G. Lohr, V. A. Adalsteinsson, K. Cibulskis, A. D. Choudhury, M. Rosenberg, P. Cruz-Gordillo, J. M. Francis, C.-Z. Zhang, A. K. Shalek, R. Satija, J. J. Trombetta, D. Lu, N. Tallapragada, N. Tahirova, S. Kim, B. Blumenstiel, C. Sougnez, A. Lowe, B. Wong, D. Auclair, E. M. Van Allen, M. Nakabayashi, R. T. Lis, G.-S. M. Lee, T. Li, M. S. Chabot, A. Ly, M.-E. Taplin, T. E. Clancy, M. Loda, A. Regev, M. Meyerson, W. C. Hahn, P. W. Kantoff, T. R. Golub, G. Getz, J. S. Boehm, and J. C. Love, "Whole-exome sequencing of circulating tumor cells provides a window into metastatic prostate cancer," *Nat. Biotechnol.*, vol. 32, no. 5, pp. 479–484, Apr. 2014.

[77] M. Yu, S. Stott, M. Toner, S. Maheswaran, and D. A. Haber, "Circulating tumor cells: approaches to isolation and characterization," *J Cell Biol*, vol. 192, no. 3, pp. 373–382, Feb. 2011.

[78] E. Ozkumur, A. M. Shah, J. C. Ciciliano, B. L. Emmink, D. T. Miyamoto, E. Brachtel, M. Yu, P. I. Chen, B. Morgan, J. Trautwein, A. Kimura, S. Sengupta, S. L. Stott, N. M. Karabacak, T. A. Barber, J. R. Walsh, K. Smith, P. S. Spuhler, J. P. Sullivan, R. J. Lee, D. T. Ting, X. Luo, A. T. Shaw, A. Bardia, L. V. Sequist, D. N. Louis, S. Maheswaran, R. Kapur, D. A. Haber, and M. Toner, "Inertial Focusing for Tumor Antigen-Dependent and -Independent Sorting of Rare Circulating Tumor Cells," *Sci. Transl. Med.*, vol. 5, no. 179, p. 179ra47, Apr. 2013.

[79] G. Vona, A. Sabile, M. Louha, V. Sitruk, S. Romana, K. Schütze, F. Capron, D. Franco, M. Pazzagli, M. Vekemans, B. Lacour, C. Bréchot, and P. Paterlini-Bréchot, "Isolation by Size of Epithelial Tumor Cells," *Am J Pathol.*, vol. 156, no. 1, pp. 57–63, Jan. 2000.

[80] I. Desitter, B. S. Guerrouahen, N. Benali-Furet, J. Wechsler, P. A. Janne, Y. Kuang, M. Yanagita, L. Wang, J. A. Berkowitz, R. J. Distel, and Y. E. Cayre, "A new device for rapid isolation by size and characterization of rare circulating tumor cells," *Anticancer*

Res, vol. 31, no. 2, pp. 427–441, Feb. 2011.

[81] J. H. Choi, A. O. Ogunniyi, M. Du, M. Du, M. Kretschmann, J. Eberhardt, and J. C. Love, "Development and optimization of a process for automated recovery of single cells identified by microengraving," *Biotechnol. Prog.*, vol. 26, no. 3, pp. 888–895, May 2010.

[82] S. P. Perfetto, P. K. Chattopadhyay, and M. Roederer, "Seventeen-colour flow cytometry: unravelling the immune system," *Nat Rev Immunol*, vol. 4, no. 8, pp. 648–655, Aug. 2004.

[83] S. C. Bendall, E. F. Simonds, P. Qiu, E.-A. D. Amir, P. O. Krutzik, R. Finck, R. V. Bruggner, R. Melamed, A. Trejo, O. I. Ornatsky, R. S. Balderas, S. K. Plevritis, K. Sachs, D. Pe'er, S. D. Tanner, and G. P. Nolan, "Single-cell mass cytometry of differential immune and drug responses across a human hematopoietic continuum," *Science*, vol. 332, no. 6030, pp. 687–696, May 2011.

[84] T. M. Gierahn, A. Yalcin, K. Shekhar, K. Ushey, S. Cu-Uvin, D. S. Kwon, R. Gottardo, B. L. Shacklett, and J. C. Love, "Multi-Spectral Image Cytometry (MuSIC) for deep phenotyping of sparse cells," *submitted*.

[85] A. H. Talasaz, A. A. Powell, D. E. Huber, J. G. Berbee, K.-H. Roh, W. Yu, W. Xiao, M. M. Davis, R. F. Pease, M. N. Mindrinos, S. S. Jeffrey, and R. W. Davis, "Isolating highly enriched populations of circulating epithelial cells and other rare cells from blood using a magnetic sweeper device," *PNAS*, vol. 106, no. 10, pp. 3970–3975, Mar. 2009.

[86] M. Vaezi, H. Seitz, and S. Yang, "A review on 3D micro-additive manufacturing technologies," *Int J Adv Manuf Technol*, vol. 67, no. 5, pp. 1721–1754, Jul. 2013.